iScience

CellPress
OPEN ACCESS

Article

Efficient antigen delivery by dendritic cell-targeting peptide via nucleolin confers superior vaccine effects in mice

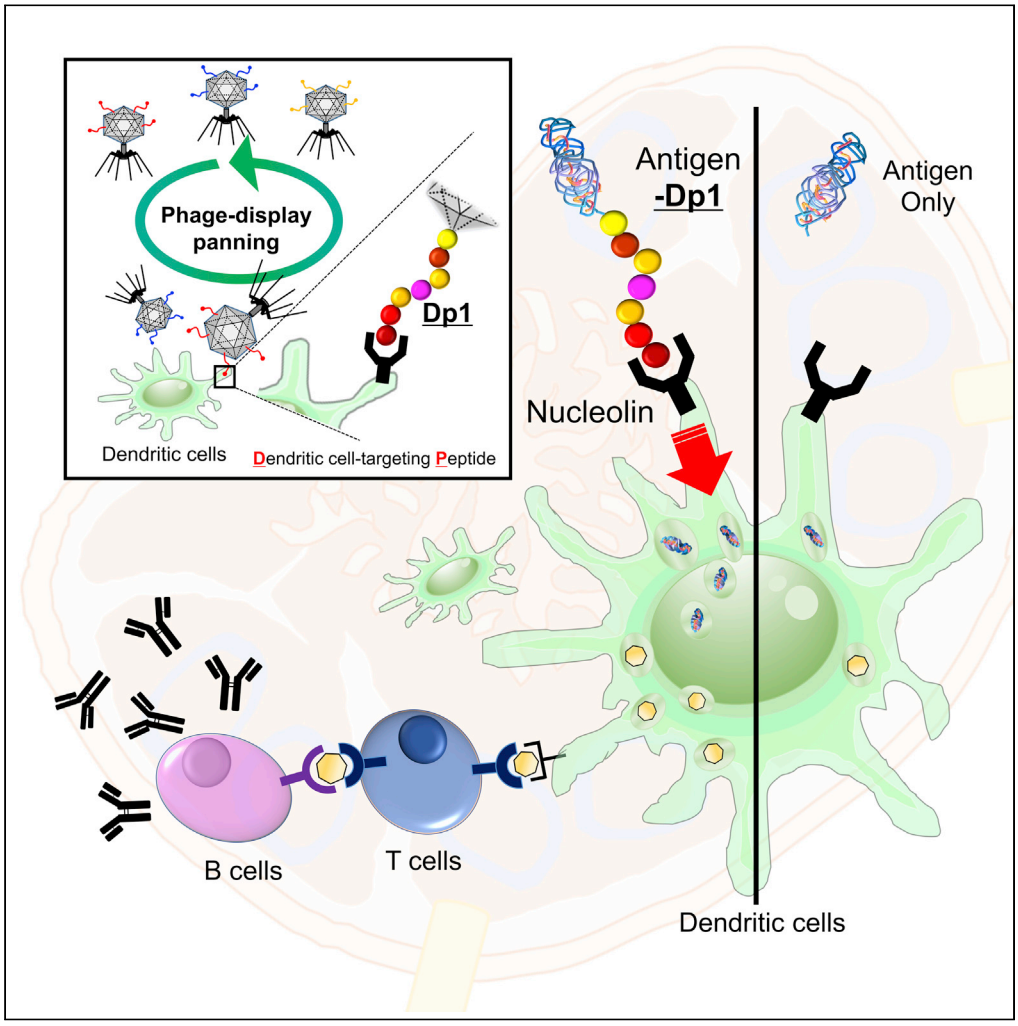

Teppei Matsuda, Kazuki Misato, Shigeyuki Tamiya, ..., Takuya Yamamoto, Michiko N. Fukuda, Yasuo Yoshioka

y-yoshioka@biken.osaka-u.ac.jp

Highlights

We successfully identified an efficient DC-targeting peptide using a phage display system

Fusion of the peptide improves the efficacy of vaccine even in the absence of adjuvants

The peptide improves the distribution of antigens to DCs and antigen presentation by DCs

Nucleolin is indispensable for the vaccine effect of the DC-targeting peptide

Matsuda et al., iScience 25, 105324
November 18, 2022
https://doi.org/10.1016/j.isci.2022.105324

iScience

CellPress
OPEN ACCESS

Article

Efficient antigen delivery by dendritic cell-targeting peptide via nucleolin confers superior vaccine effects in mice

Teppei Matsuda,[1,2,3,15] Kazuki Misato,[1,2,3,15] Shigeyuki Tamiya,[1,2,3,15] Yasuhiro Akeda,[4,5] Ikuhiko Nakase,[6,7] Etsushi Kuroda,[8] Shokichi Takahama,[9] Motohiro Nonaka,[10] Takuya Yamamoto,[9] Michiko N. Fukuda,[11] and Yasuo Yoshioka[1,2,3,12,13,14,16,*]

SUMMARY

Efficient delivery of subunit vaccines to dendritic cells (DCs) is necessary to improve vaccine efficacy, because the vaccine antigen alone cannot induce sufficient protective immunity. Here, we identified DC-targeting peptides using a phage display system and demonstrated the potential of these peptides as antigen-delivery carriers to improve subunit vaccine effectiveness in mice. The fusion of antigen proteins and peptides with DC-targeting peptides induced strong antigen-specific IgG responses, even in the absence of adjuvants. In addition, the DC-targeting peptide improved the distribution of antigens to DCs and antigen presentation by DCs. The combined use of an adjuvant with a DC-targeting peptide improved the effectiveness of the vaccine. Furthermore, nucleolin, located on the DC surface, was identified as the receptor for DC-targeting peptide, and nucleolin was indispensable for the vaccine effect of the DC-targeting peptide. Overall, the findings of this study could be useful for developing subunit vaccines against infectious diseases.

INTRODUCTION

As evidenced by the recent COVID-19 and influenza pandemics, infectious diseases caused by several types of pathogens are a serious challenge for global health. Vaccines are the most efficient preventive measures against infectious diseases because they can reduce the severity of clinical symptoms and limit the spread of infections (Delany et al., 2014; Graham and Sullivan, 2018; Pardi et al., 2018). In addition, vaccines could be potential therapeutics against cancer, nervous system disorders, and metabolic diseases (Kobiyama et al., 2019; Malonis et al., 2020; Saxena et al., 2021). Presently, there are several types of vaccines against infectious diseases, including attenuated live virus vaccines, inactivated whole virus vaccines, messenger RNA vaccines, virus vector-based vaccines, and protein- or peptide-based subunit vaccines (Cid and Bolivar, 2021; Delany et al., 2014; Pardi et al., 2018; Plotkin, 2009). Each of these vaccine types possess specific advantages and disadvantages. For instance, subunit vaccines, which use pathogen-derived proteins or peptides as vaccine antigens, have several advantages, including superior safety, negligible chance of mutation within the target-expressed gene, easy upscaling of production, low-cost of production, and easy storage requirements (Cid and Bolivar, 2021; Krammer, 2019). However, subunit vaccines evoke only weak adaptive immunity, such as pathogen-specific antibody responses. To induce strong adaptive immunity against pathogens, dendritic cells (DCs), which are antigen-presenting cells (APCs), must capture vaccine antigens for efficient activation (Eisenbarth, 2019). Therefore, the rational use of adjuvants to activate DCs and antigen-delivery carriers to efficiently deliver vaccine antigens to DCs can help improve the effectiveness of subunit vaccines (Tacken and Figdor, 2011).

Currently, several adjuvants have been developed in preclinical and clinical studies (Del Giudice et al., 2018). For example, aluminum salts (alum) are some of the most reliable adjuvants, with several vaccines formulated using them (HogenEsch et al., 2018). In addition, oligodeoxynucleotides (ODNs) with unmethylated cytosine-phosphate-guanine (CpG) motifs (CpG ODNs), which are short single-stranded synthetic DNA fragments containing immunostimulatory CpG motifs and toll-like receptor (TLR) 9 agonist, is one of the most effective adjuvants for inducing antibody and Th1-type immune responses (Shirota and

[1]Laboratory of Nano-design for Innovative Drug Development, Graduate School of Pharmaceutical Sciences, Osaka University, 1-6 Yamadaoka, Suita, Osaka 565-0871, Japan

[2]Vaccine Creation Group, BIKEN Innovative Vaccine Research Alliance Laboratories, Institute for Open and Transdisciplinary Research Initiatives, Osaka University, 3-1 Yamadaoka, Suita, Osaka 565-0871, Japan

[3]Vaccine Creation Group, BIKEN Innovative Vaccine Research Alliance Laboratories, Research Institute for Microbial Diseases, Osaka University, 3-1 Yamadaoka, Suita, Osaka 565-0871, Japan

[4]Department of Bacteriology I, National Institute of Infectious Diseases, 1-23-1 Toyama, Shinjuku, Tokyo 162-8640, Japan

[5]Japan-Thailand Research Collaboration Center on Emerging and Re-emerging Infections, Research Institute for Microbial Diseases, Osaka University, 3-1 Yamadaoka, Suita, Osaka 565-0871, Japan

[6]Graduate School of Science, Osaka Metropolitan University, 1-1 Gakuen-cho, Naka-ku, Sakai, Osaka 599-8531, Japan

[7]NanoSquare Research Institute, Osaka Prefecture University, 1-2 Gakuen-cho, Naka-ku, Sakai, Osaka 599-8570, Japan

[8]Department of Immunology, School of Medicine, Hyogo Medical University, 1-1 Mukogawa, Nishinomiya, Hyogo 663-8501, Japan

[9]Laboratory of Immunosenescence, Center for Vaccine & Adjuvant

Continued

Klinman, 2014). However, adjuvants can cause systemic inflammations, resulting in adjuvant-dependent adverse reactions (Heikenwalder et al., 2004; Seya et al., 2015). Therefore, the combined use of antigen-delivery carriers with adjuvants is expected to improve vaccine efficacy, with less side effects.

Several approaches have been developed for the efficient delivery of antigens to DCs (Caminschi and Shortman, 2012; Goyvaerts and Breckpot, 2015; Tacken and Figdor, 2011). One such approach involves encapsulating antigens in particle-based vehicles, such as liposomes and bio-degradable nanoparticles (20- to 100-nm), which can be preferentially trafficked into lymphatic vessels and travel toward lymph nodes (Irvine et al., 2013; Moyer et al., 2016). Another approach is the conjugation of antigens to a monoclonal antibody specific for a particular receptor on DCs, such as DEC205, CD11c, or Clec9A (Dhodapkar et al., 2014; Hossain and Wall, 2019; Idoyaga et al., 2011; Macri et al., 2016; Trumpfheller et al., 2012). For example, the delivery of tumor antigen using a monoclonal antibody against DEC205 increases the efficiency of antigen presentation on DCs and induces tumor antigen-specific immune responses in cancer patients (Dhodapkar et al., 2014). Although this strategy is useful, its application has several limitations (Dhodapkar et al., 2014; Hossain and Wall, 2019; Idoyaga et al., 2011; Macri et al., 2016; Trumpfheller et al., 2012). For instance, because mouse-derived antibodies are generally used in preclinical studies, they must be humanized for human use. In addition, there is a need to improve the existing method for chemical conjugation of antigens with antibodies. Moreover, human monoclonal antibodies exhibit antigenicity and may often induce antibodies against therapeutic monoclonal antibodies (Beerli and Rader, 2010). In contrast to monoclonal antibodies, peptides have low antigenicity and the fusion of peptides to specific proteins is easy, indicating that DC-targeting peptides might be effective carriers for antigen delivery (Gou et al., 2021; Sioud et al., 2013; Yan et al., 2016). Moreover, previous studies have shown that the fusion of Clec9-specific peptides and peptide antigens efficiently induces antigen-specific $CD8^+$T cell responses (Gou et al., 2021; Yan et al., 2016). However, the functions and mechanisms of DC-targeting peptides remain poorly understood because of the difficulty in obtaining DC-targeting peptides. Particularly, it remains unclear whether the fusion of DC-targeting peptides and antigens improves antigen-specific antibody responses *in vivo*.

One of the technologies for the identification and screening of desired DC-targeting peptides for the development of subunit vaccines is the phage display system. The phage display system is an unbiased high-throughput screening technique for identifying desired functional peptides that target specific proteins or cells (Hoogenboom et al., 1998; Mukai et al., 2005; Teesalu et al., 2012). One of the advantages of this system is the large peptide library size, which contains as many as 10^9 different peptides. In addition, this system makes it possible to obtain peptides for specific proteins, whole cells, and tissues without *a priori* knowledge of the targets or their concentrations. This system has been successfully used to identify peptide ligands specific to cancer cells, macrophages, organ vasculature, and tumor vasculature (Fukuda et al., 2000; Mann et al., 2016; Scodeller et al., 2017; Sugihara et al., 2014).

Therefore, the aim of this study was to develop a DC-targeting peptide for vaccine delivery against infectious diseases. To achieve this, we identified an efficient DC-targeting peptide using a phage display system and evaluated the potential of this DC-targeting peptide for the delivery of subunit vaccines to mice. The findings of this study could be important for the development of an effective carrier for vaccines against infectious diseases.

RESULTS

Identification of DC-targeting peptides using a phage display system

To identify DC-targeting peptide (Dp), a T7 phage-based library displaying 7-mer linear peptides was mixed with EL4 cells, a mouse T-cell lymphoma cell line, and B16-F10 cells, which is a mouse melanoma cell line. Phages that did not bind to these cells were recovered and then mixed with mouse bone marrow-derived DCs (BMDCs). Phages that could bind to BMDCs were recovered and amplified through infection with *E. coli*, and three rounds of selection were performed. Overall, the number of phage clones that bound to the BMDCs relative to the total number of added phages increased with each round of selection (Figure 1A). Thereafter, the BMDC binding ability of purified single-phage clones was assessed using flow cytometry. Among approximately 200 randomly selected phage clones, 40 different phage clones with BMDC-binding ability were identified (Figures 1B and S1), and the results of the representative clones are shown in Figure 1B; the remainder of the phage clones did not exhibit BMDC-binding activity (Figure S2). Analysis of the peptide sequences using DC-binding phage clones revealed that most peptides

Research, National Institutes of Biomedical Innovation, Health and Nutrition, 7-6-8 Saito-Asagi, Ibaraki, Osaka 567-0085, Japan

[10]Department of Biological Chemistry, Human Health Sciences, Graduate School of Medicine, Kyoto University, 53 kawahara-cho, Shogoin, Sakyo-ku, Kyoto 606-8507, Japan

[11]Cancer Center, Sanford-Burnham-Prebys Medical Discovery Institute, 10901 North Torrey Pines Road, La Jolla, CA 92037, USA

[12]The Research Foundation for Microbial Diseases of Osaka University, 3-1 Yamadaoka, Suita, Osaka 565-0871, Japan

[13]Global Center for Medical Engineering and Informatics, Osaka University, 3-1 Yamadaoka, Suita, Osaka 565-0871, Japan

[14]Center for Infectious Disease Education and Research (CiDER), Osaka University, 2-8 Yamadaoka, Suita, Osaka 565-0871, Japan

[15]These authors contributed equally

[16]Lead contact

*Correspondence: y-yoshioka@biken.osaka-u.ac.jp

https://doi.org/10.1016/j.isci.2022.105324

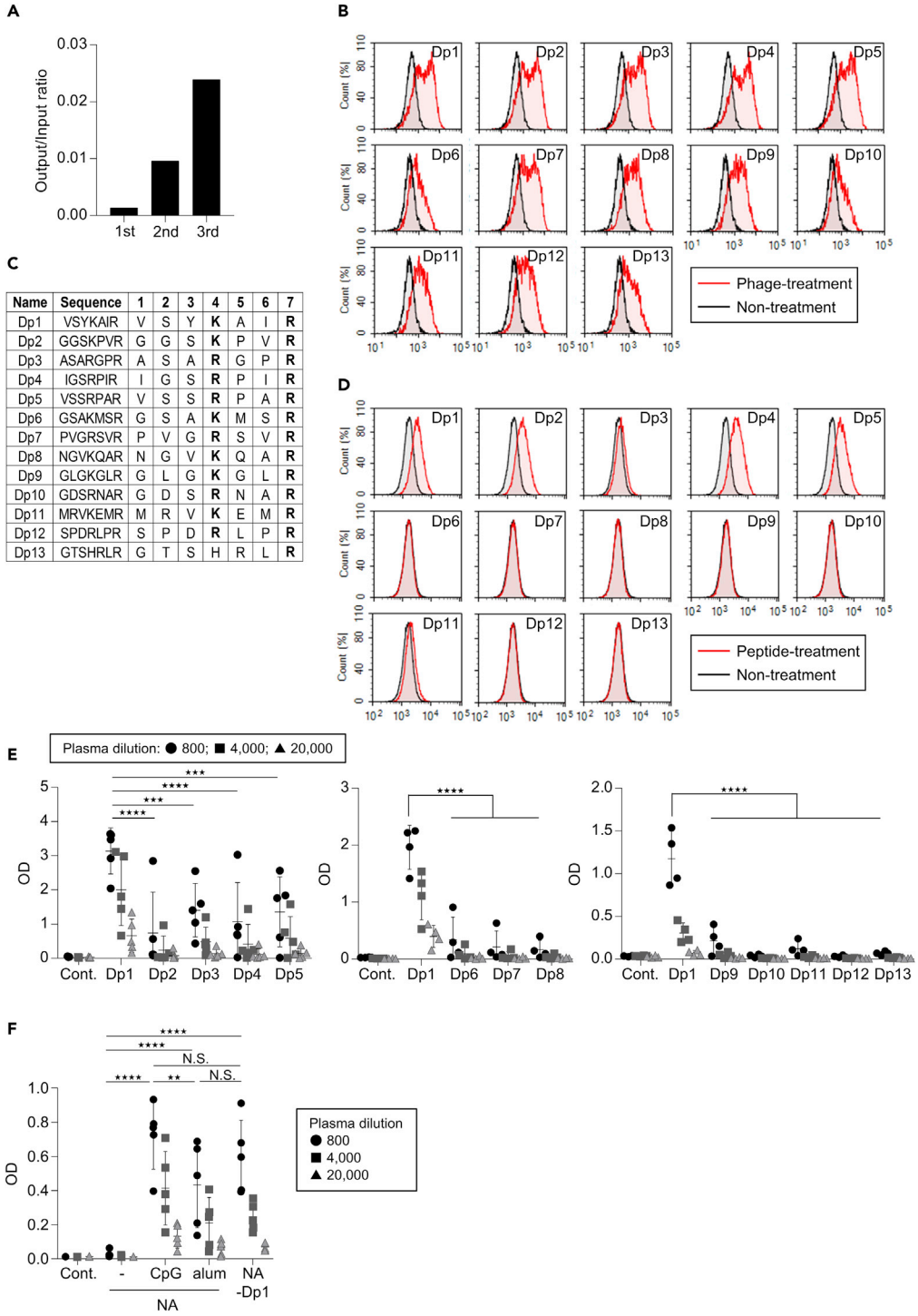

Name	Sequence	1	2	3	4	5	6	7
Dp1	VSYKAIR	V	S	Y	**K**	A	I	**R**
Dp2	GGSKPVR	G	G	S	**K**	P	V	**R**
Dp3	ASARGPR	A	S	A	**R**	G	P	**R**
Dp4	IGSRPIR	I	G	S	**R**	P	I	**R**
Dp5	VSSRPAR	V	S	S	**R**	P	A	**R**
Dp6	GSAKMSR	G	S	A	**K**	M	S	**R**
Dp7	PVGRSVR	P	V	G	**R**	S	V	**R**
Dp8	NGVKQAR	N	G	V	**K**	Q	A	**R**
Dp9	GLGKGLR	G	L	G	**K**	G	L	**R**
Dp10	GDSRNAR	G	D	S	**R**	N	A	**R**
Dp11	MRVKEMR	M	R	V	**K**	E	M	**R**
Dp12	SPDRLPR	S	P	D	**R**	L	P	**R**
Dp13	GTSHRLR	G	T	S	H	R	L	**R**

Figure 1. Identification of DC-targeting peptides by phage display system

(A) The number of phage clones recovered from mouse-derived BMDCs (output) relative to the total number of added phage (input) at each selection round.

(B) The binding of each phage clone from the third round of selection to BMDCs was evaluated using flow cytometry.

(C) Peptide sequences displayed by selected phage clones with binding capacity to BMDCs.

(D) The binding of each biotin-labeled DC-targeting peptide to BMDCs was detected by fluorescent-labeled streptavidin using flow cytometry.

Figure 1. *Continued*

(E and F) Mice were immunized with (E) 5 μg neutravidin (NA) and 5 μg DC-targeting peptides complex, and (F) 5 μg NA alone, 5 μg NA plus 10 μg CpG ODN, 5 μg NA plus 250 μg alum, or 5 μg NA and Dp1 (NA-Dp1) complex. As control, mice were treated with PBS. Level of NA-specific IgG in plasma were evaluated 7 days after the second immunization using ELISA.

(E and F) We used 800- (●), 4,000- (■), and 20,000- (▲) fold–diluted plasma samples. (E) $n = 4–5$; (F) $n = 5$. (E and F) Data are means ± SD. **p< 0.01, ***p< 0.001, ****p< 0.0001 as indicated by Tukey's test. N.S.: not significant. Significant differences were analyzed only in the 800-fold-diluted plasma samples. See also Figures S1 and S2.

contained consensus sequences with arginine and lysine residues at the 4th and 7th positions, called the R/K-X-X-R motif (where, R is arginine, K is lysine, and X is any amino acid) (Figure 1C). Next, we examined the BMDC-binding ability of these peptides using synthetic peptides. Some peptides, such as Dp1, Dp2, Dp4, and Dp5, exhibited strong binding to BMDCs (Figure 1D). In contrast, the other peptides did not bind to BMDCs because of their low sensitivity (Figure 1D), although the phage assay indicated that these peptides should bind to BMDCs (Figure 1B). These results indicate that some peptides with the R/K-X-X-R motif at the C-terminus can bind efficiently to DCs.

Potential of DC-targeting peptides as an antigen-delivery carrier

Neutravidin, a derivative of streptavidin, was used as a model antigen to examine the potential of the identified DC-targeting peptide as an antigen-delivery carrier. Each DC-targeting peptide labeled with biotin was mixed with neutravidin, and the purified complex was used as a vaccine antigen. Therefore, the purified complex contains one molecule of neutravidin and four molecules of DC-targeting peptide. Mice were immunized with a complex of biotin-labeled peptide and neutravidin twice subcutaneously, and the level of neutravidin-specific IgG in their plasma was determined using ELISA. The level of neutravidin-specific IgG in neutravidin-Dp1–immunized mice was significantly higher than that of the other neutravidin-peptides (Figure 1E), although the peptides contained the same R/K-X-X-R motif (Figure 1C). To examine the strength of the immune responses induced by Dp1, we used alum and CpG ODN as adjuvants. Although neutravidin-immunized mice did not induce neutravidin-specific IgG, neutravidin plus CpG ODN-, and neutravidin plus alum-immunized mice showed a strong level of neutravidin-specific IgG (Figure 1F). The levels of neutravidin-specific IgG in the neutravidin-Dp1–immunized mice were comparable to those in the neutravidin plus CpG ODN- and neutravidin plus alum-immunized mice (Figure 1F). These data demonstrated that Dp1 can induce strong antigen-specific IgG, even in the absence of an adjuvant.

Application of Dp1 for vaccine against *Streptococcus pneumoniae*

To verify the potential of Dp1 as an antigen-delivery carrier, we used pneumococcal surface protein A (PspA) as an antigen for a vaccine against *Streptococcus pneumoniae*. Because PspA is expressed on several *S. pneumoniae* isolates and induces cross-reactivity among different strains, it is considered an ideal antigen for the development of pneumococcal vaccines (Khan and Jan, 2017; Masomian et al., 2020). We genetically fused three peptides Dp1 (Dp1×3) or other peptides such as Dp2 (Dp2×3) and Dp3 (Dp3×3) to the C-terminal of PspA, and recombinant PspA-peptide proteins were produced using *E. coli*. Mice were immunized with wild-type (WT) PspA in the presence or absence of alum or CpG ODN, or with PspA-peptide twice subcutaneously. WT PspA in combination with alum or CpG ODN induced significantly higher plasma PspA-specific IgG levels compared to WT PspA alone (Figure 2A). Furthermore, immunization with PspA-Dp1×3 induced strong PspA-specific IgG levels comparable to PspA plus CpG ODN; however, PspA plus alum induced significantly higher PspA-specific IgG levels than PspA-Dp1×3 (Figure 2A). In contrast, PspA-Dp2×3 and PspA-Dp3×3 did not induce plasma PspA-specific IgG levels (Figure 2B). In addition, we used another mouse strain, namely BALB/c, to examine the usefulness of PspA-Dp1×3. We observed that immunization with PspA-Dp1×3 induced plasma PspA-specific IgG levels comparable to those induced with WT PspA plus alum in BALB/c mice (Figure 2C). However, immunization with PspA-Dp1×3 did not induce Dp1×3-specific IgG, indicating that Dp1×3 has low antigenicity (Figure 2D). To evaluate whether the PspA-specific IgG response induced by PspA-Dp1×3 was sufficient to protect against pneumococcal infection, mice were challenged with *S. pneumoniae* after the second immunization, and the weight loss and survival rate of the mice after the challenge was examined. The body weight and survival rate of non-immunized control mice, WT PspA-immunized mice, and PspA-Dp3×3–immunized mice decreased after challenge (Figures 2E and 2F). Particularly, the survival rate of WT PspA-immunized and PspA-Dp3×3–immunized mice was approximately 30% and 40%, respectively (Figure 2F). In contrast, there was no significant decrease in the body weight and survival rate of WT

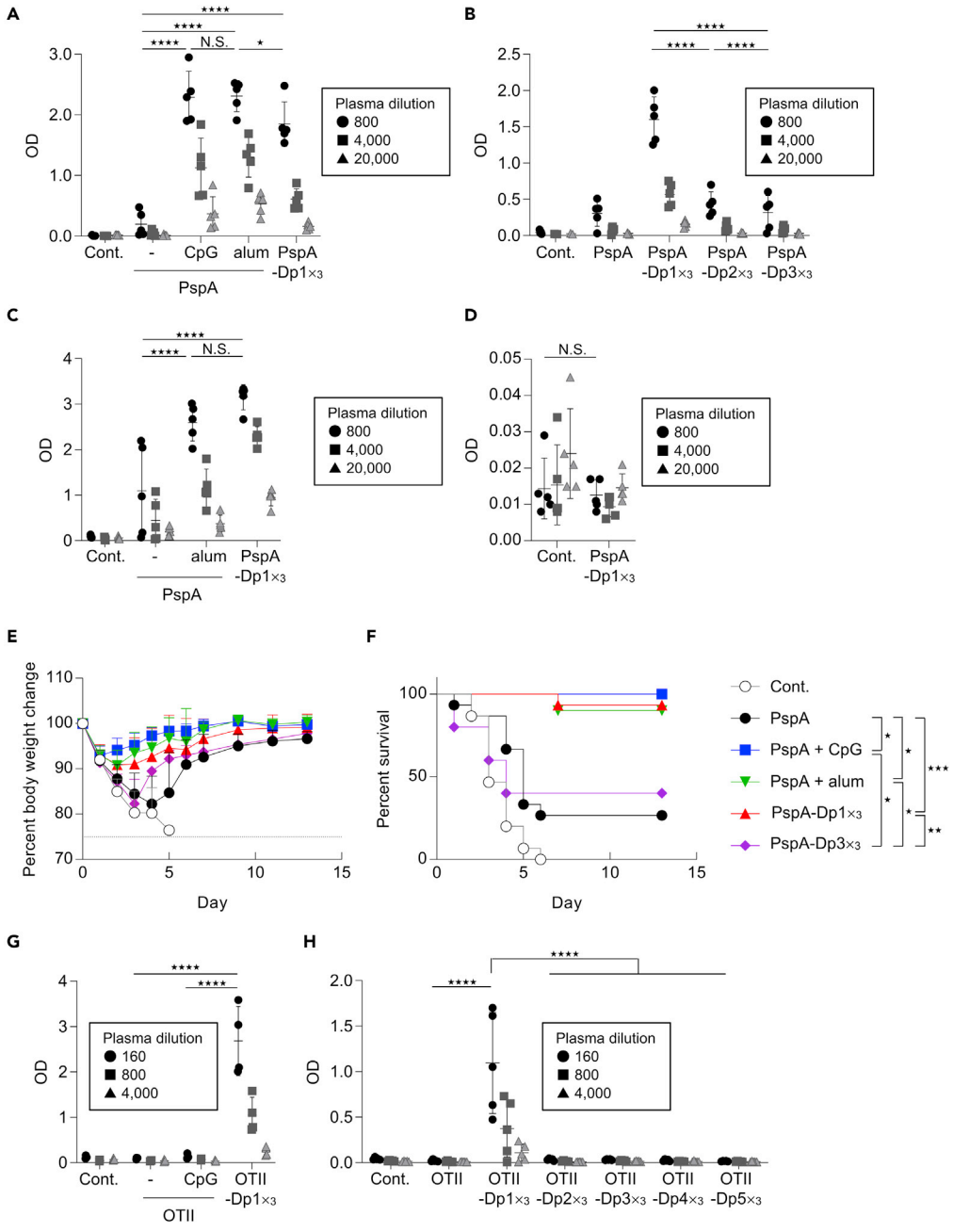

Figure 2. Potential of Dp1as an antigen-delivery carrier for vaccine against *Streptococcus pneumoniae*

(A, B, and D–F) C57BL/6J mice or (C) BALB/c mice were immunized with 1 μg PspA alone, 1 μg PspA plus 10 μg CpG ODN, 1 μg PspA plus 50 μg alum, 1 μg PspA-Dp1×3, 1 μg PspA-Dp2×3, or 1 μg PspA-Dp3×3. Plasma levels of (A–C) PspA-specific IgG and (D) Dp1×3-specific IgG were evaluated 7 days after the second immunization using ELISA.

(A–D) We used 800- (●), 4,000- (■), and 20,000- (▲) fold–diluted plasma samples.

(E and F) At 10 days after the second immunization, C57BL/6J mice were challenged with *Streptococcus pneumoniae*. Percentage change in (E) initial body weight and (F) survival were monitored after challenge.

(G and H) Mice were immunized with 1.1 nmol (equivalent to 2 μg) OTII alone, 1.1 nmol (equivalent to 2 μg) OTII plus 50 μg CpG ODN, 1.1 nmol (equivalent to 5 μg) OTII-Dp1×3, or 1.1 nmol (equivalent to 5 μg) fusion OTII with the other peptides. Plasma level of OVA-specific IgG were evaluated 7 days after the second immunization using ELISA. We used 160- (●), 800- (■), and 4,000- (▲) fold–diluted plasma samples.

(A–D and H) $n = 5$; (E and F) $n = 5$–15; (G) $n = 4$.

Figure 2. *Continued*
(A–E, G, and H) Data are means ± SD. *p< 0.05, ****p< 0.0001 as indicated by Tukey's test. N.S.: not significant. Significant differences were analyzed only in the (A–D) 800-fold-diluted and (G and H) 160-fold–diluted plasma samples. (F) *p< 0.05, **p< 0.01, ***p< 0.001 as indicated by comparing Kaplan-Meier curves using the log-rank test. See also Figure S3.

PspA plus alum-immunized and PspA-Dp1×3-immunized mice (Figures 2E and 2F). Moreover, immunization with PspA-Dp1×3, WT PspA plus CpG ODN, or WT PspA plus alum, protected the mice against pneumococcal infection even after the first immunization (Figure S3). Overall, these findings suggest that immunization with PspA-Dp1×3 can induce PspA-specific antibody response that is sufficient to protect against pneumococcal infection, even in the absence of an adjuvant.

To confirm the versatility of Dp1 against various types of antigens, we used a peptide from ovalbumin (OVA) as an antigen. The peptide from aa323-339 of OVA (OTII) is an MHC class II epitope in mice, and it is known that antibodies to this peptide are also induced in mice. OTII with Dp1×3 (OTII-Dp1×3) was synthesized chemically, and mice were immunized with OTII-Dp1×3 twice. Immunization with OTII-Dp1×3 induced significantly higher plasma OVA-specific IgG levels compared with mice immunized with the control, even in the absence of adjuvant (Figure 2G). However, immunization with OTII plus CpG ODN did not induce plasma OVA-specific IgG levels (Figure 2G). Fusion of OTII with the other peptides did not induce OVA-specific IgG (Figure 2H). These data suggest that Dp1 could be applied to various types of antigens, such as proteins and peptides.

Combined effect of Dp1 with an adjuvant

Furthermore, we examined the combined effect of PspA-Dp1×3 and CpG ODN as an adjuvant. The levels of PspA-specific total IgG and IgG2c in PspA-Dp1×3 plus CpG ODN-immunized mice were significantly higher than those in WT PspA plus CpG ODN- and PspA-Dp1×3-immunized mice (Figure 3A), and there was no significant difference in the PspA-specific IgG1 levels of mice immunized with WT PspA plus CpG ODN, PspA-Dp1×3, and PspA-Dp1×3 plus CpG ODN (Figure 3A). Next, we examined the long-term persistence of PspA-specific total IgG in the plasma after immunization. Five months after immunization, the retention rate of PspA-specific total IgG in PspA-Dp1×3–immunized mice was higher than that in WT PspA plus CpG ODN-immunized mice (Figure 3B). Furthermore, PspA-Dp1×3 plus CpG ODN-immunized mice showed a significantly higher retention rate of PspA-specific total IgG than WT PspA plus CpG ODN-immunized mice (Figure 3B). To investigate PspA-specific $CD4^+$T cell responses, splenocytes from immunized mice were stimulated with WT PspA *in vitro*, and the level of IFN-γ in the supernatant was determined. The IFN-γ level of PspA-Dp1×3 plus CpG ODN-immunized mice were significantly higher than that of WT PspA-, WT PspA plus CpG ODN-, and PspA-Dp1×3-immunized mice (Figure 3C). Moreover, CpG ODN-adjuvanted OTII-Dp1×3 induced significantly higher levels of OVA-specific total IgG and IgG2c than OTII-Dp1×3 (Figure 3D). These results suggest that the combined use of Dp1 and adjuvants such as CpG ODN could improve antibody production and T cell responses.

Rational design of Dp1 as an antigen-delivery carrier

In this study, we examined the properties of Dp1 as an antigen-delivery carrier. First, we investigated the optimal number of Dp1 for fusion with the antigen to induce antigen-specific antibody responses; we used PspA-Dp1×3 and OTII-Dp1×3 containing three molecules of Dp1, as shown in Figures 2 and 3. The results showed that immunization with PspA-Dp1 containing one or two molecules of Dp1 (PspA-Dp1 or PspA-Dp1×2, respectively) did not induce plasma PspA-specific IgG or protect mice against pneumococcal challenge compared to immunization with PspA-Dp1×3 (Figures 4A and 4B). Moreover, OTII containing a single Dp1 (OTII-Dp1) did not induce OVA-specific IgG (Figure 4C).

Furthermore, we examined the importance of Dp1×3 fusion site on PspA. PspA with Dp1×3 fused to the N-terminal did not induce PspA-specific IgG compared with PspA with Dp1×3 fused to the C-terminal (Figure 4D). The results suggest that the exposure of the C-terminal of Dp1×3 might be important for inducing antigen-specific immune responses. To further assess the role of C-terminal of Dp1×3, we examined whether the addition of alanine residues to the C-terminal of Dp1×3 affects immune responses induced by Dp1×3. The addition of two alanine residues to the C-terminal of PspA-Dp1×3 could not induce PspA-specific IgG (Figure 4D), suggesting the importance of the exposure of C-terminal of Dp1×3 in inducing immune responses. Next, we compared the potential of Dp1 as an antigen-delivery carrier using

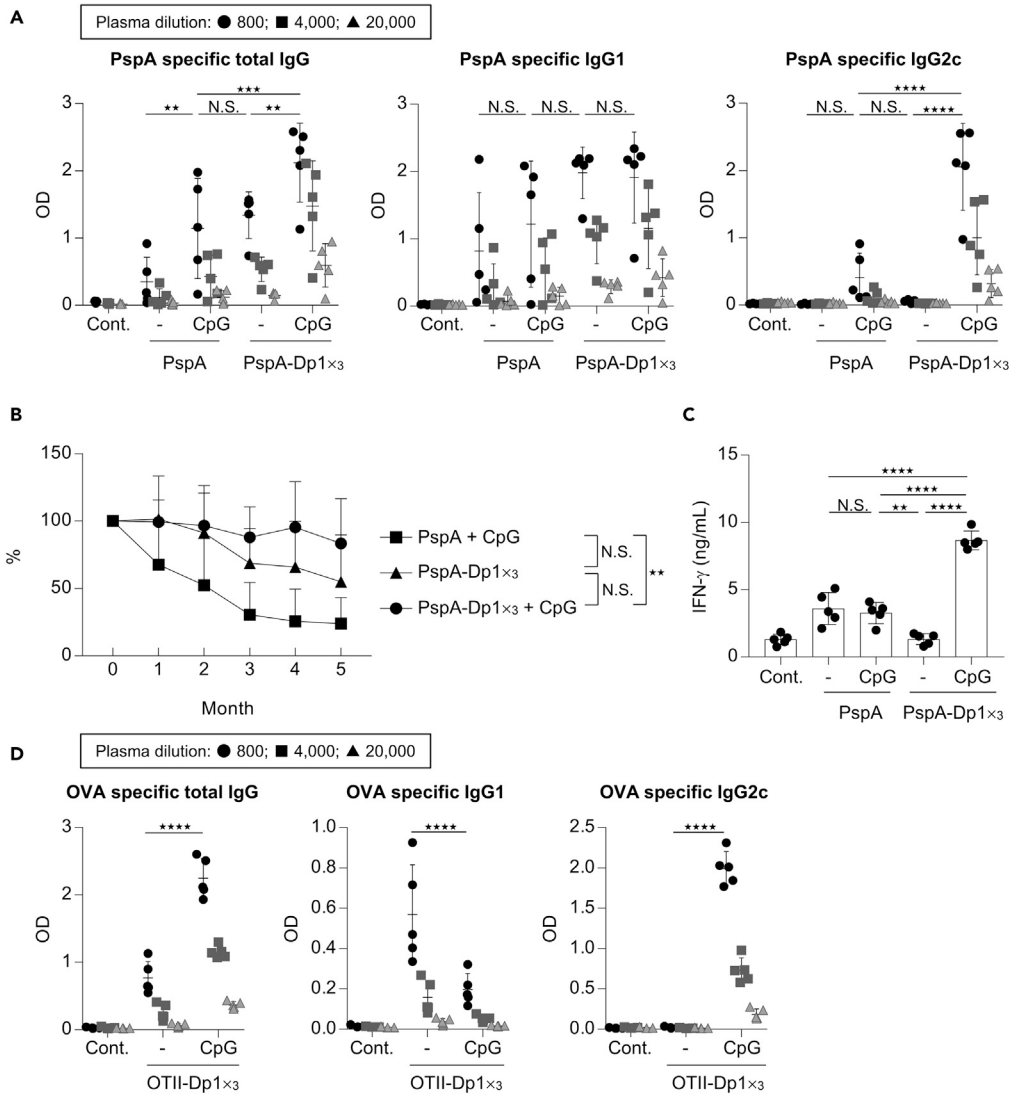

Figure 3. Combined effect of Dp1 with adjuvant

(A–C) Mice were immunized with 1 μg PspA or 1 μg PspA-Dp1×3 with or without 10 μg CpG ODN.

(A) Levels of PspA-specific total IgG, IgG1, and IgG2c in plasma were evaluated 7 days after the second immunization using ELISA.

(B) Several months later after the second immunization, the level of PspA-specific total IgG in plasma was evaluated using ELISA. We used 800-fold–diluted plasma samples.

(C) At 7 days after the second immunization, splenocytes obtained from immunized mice were incubated in the presence of PspA *in vitro* and the level of IFN-γ in the supernatant was measured after 1 day.

(D) Mice were immunized with 1.1 nmol (equivalent to 5 μg) OTII-Dp1×3 or 1.1 nmol (equivalent to 5 μg) OTII-Dp1×3 plus 50 μg CpG ODN. OVA-specific total IgG, IgG1, and IgG2c in plasma were evaluated using ELISA at 7 days after the second immunization.

(A and D) We used 800- (●), 4,000- (■), and 20,000- (▲) fold–diluted plasma samples. (A–D) $n = 5$. Data are means ± SD. **p< 0.01, ***p< 0.001, ****p< 0.0001 as indicated by Tukey's test. N.S.: not significant.

(A and D) Significant differences were analyzed for only the 800-fold-diluted plasma samples.

Tat peptide. The Tat peptide from human immunodeficiency virus type 1 is a representative cell-penetrating peptide that is used as a delivery carrier for proteins into cells (Lonn and Dowdy, 2015). We used PspA-Tat containing monomeric Tat peptide, but not PspA-Tat×3 containing trimeric Tat peptide, because we could not remove endotoxins from purified PspA-Tat×3. The level of PspA-specific IgG in PspA-Tat–immunized mice was significantly lower than that in PspA-Dp1×3–immunized mice (Figure 4E).

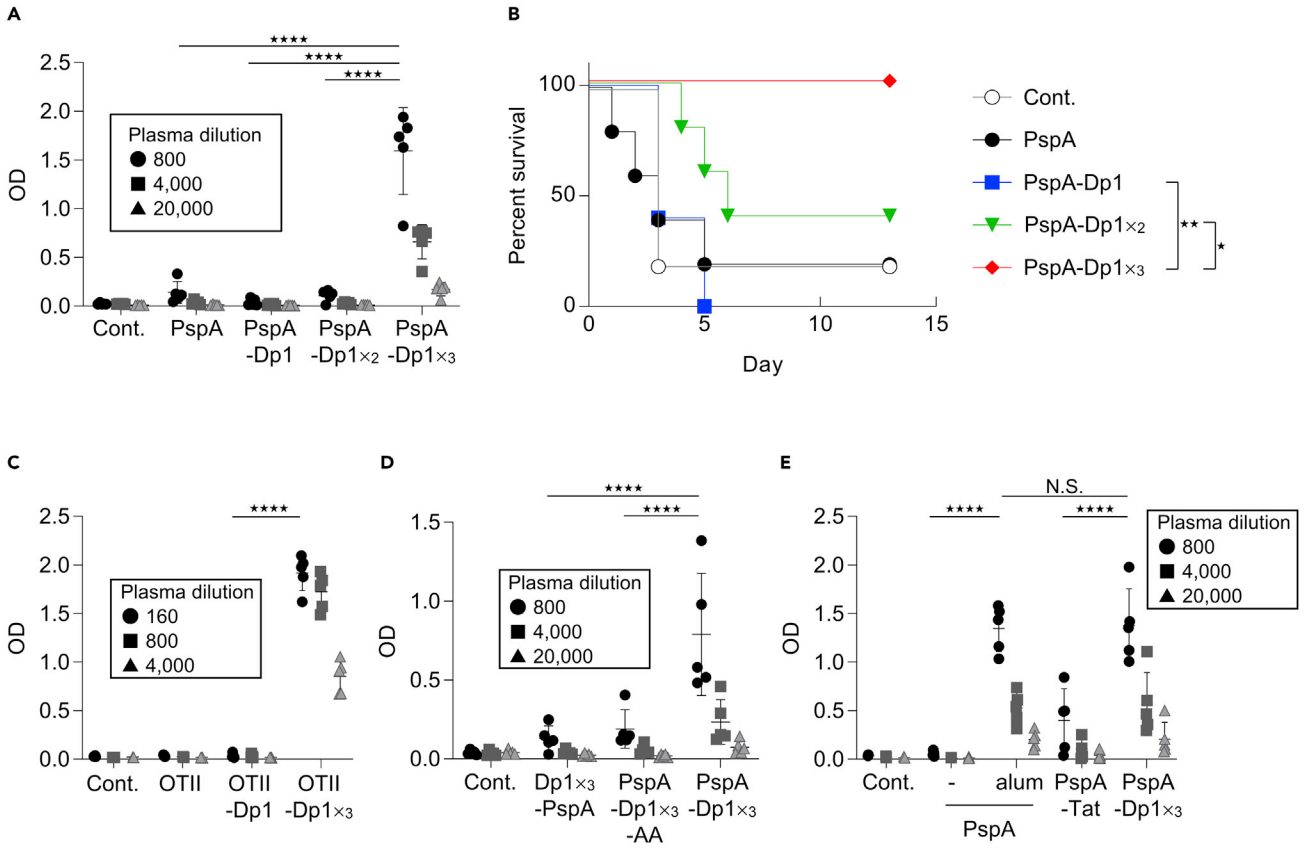

Figure 4. Rational design of Dp1 as an antigen-delivery carrier

(A and B) Mice were immunized with 1 μg PspA alone, 1 μg PspA-Dp1 which have one, two, or three Dp1 at the C-terminal.

(A) Plasma level of PspA-specific IgG was evaluated 7 days after the second immunization using ELISA.

(B) At 10 days after the second immunization, mice were challenged with *Streptococcus pneumoniae* and survival rate was monitored.

(C) Mice were immunized with 1.1 nmol (equivalent to 2 μg) OTII alone, 1.1 nmol (equivalent to 3 μg) OTII-Dp1, or 1.1 nmol (equivalent to 5 μg) OTII-Dp1×3 at the C-terminal. Plasma level of OVA-specific IgG was evaluated 7 days after the second immunization using ELISA.

(D and E) Mice were immunized with (D) 1 μg Dp1×3-PspA, 1 μg PspA-Dp1×3 with two alanine residues at the C-terminal, or 1 μg PspA-Dp1×3, and (E) 1 μg PspA alone, 1 μg PspA plus 50 μg alum, 1 μg PspA-Tat, or 1 μg PspA-Dp1×3. The level of PspA-specific IgG in the plasma samples was evaluated 7 days after the second immunization using ELISA.

(A and C–E) We used (A, D, and E) 800- (●), 4,000- (■), and 20,000- (▲) fold–diluted, and (C) 160- (●), 800- (■), and 4,000- (▲) fold–diluted plasma samples. (A–E) $n = 5$. (A and C–E) Data are presented as mean ± SD. ****$p < 0.0001$ as indicated by Tukey's test. N.S.: not significant. Significant differences were analyzed only in the (A, D, and E) 800-fold-diluted and (C) 160-fold-diluted plasma samples. (B) *$p < 0.05$, **$p < 0.01$ as indicated by comparing Kaplan-Meier curves using the log-rank test.

Overall, these results suggest that the addition of three Dp1 to the C-terminus of the antigen is necessary to induce sufficient immune responses.

Importance of Dp1 fusion with antigens

To examine the mechanism of Dp1-induced immune responses, we first determined whether Dp1 fusion to the antigen affects antibody responses. Mice were immunized with a mixture of WT PspA and free Dp1×3, and the plasma level of PspA-specific IgG was examined. The results showed that there was no significant difference in the plasma PspA-specific IgG levels of WT PspA-immunized mice and WT PspA plus free Dp1×3-immunized mice (Figure 5A). To further verify the influence of antigen fusion with Dp1, mice were immunized with OVA plus PspA-Dp1×3 or OVA plus alum, and the plasma level of OVA-specific IgG was examined. Neither OVA only nor OVA plus PspA-Dp1×3 induced OVA-specific IgG, however, OVA plus alum strongly induced OVA-specific IgG (Figure 5B). These results indicated the importance of Dp1 fusion to the antigen in inducing strong antigen-specific antibody responses. To examine the DC targeting capacity of Dp1 in enhancing immune responses, mice were immunized with OTII-Dp1×3 plus

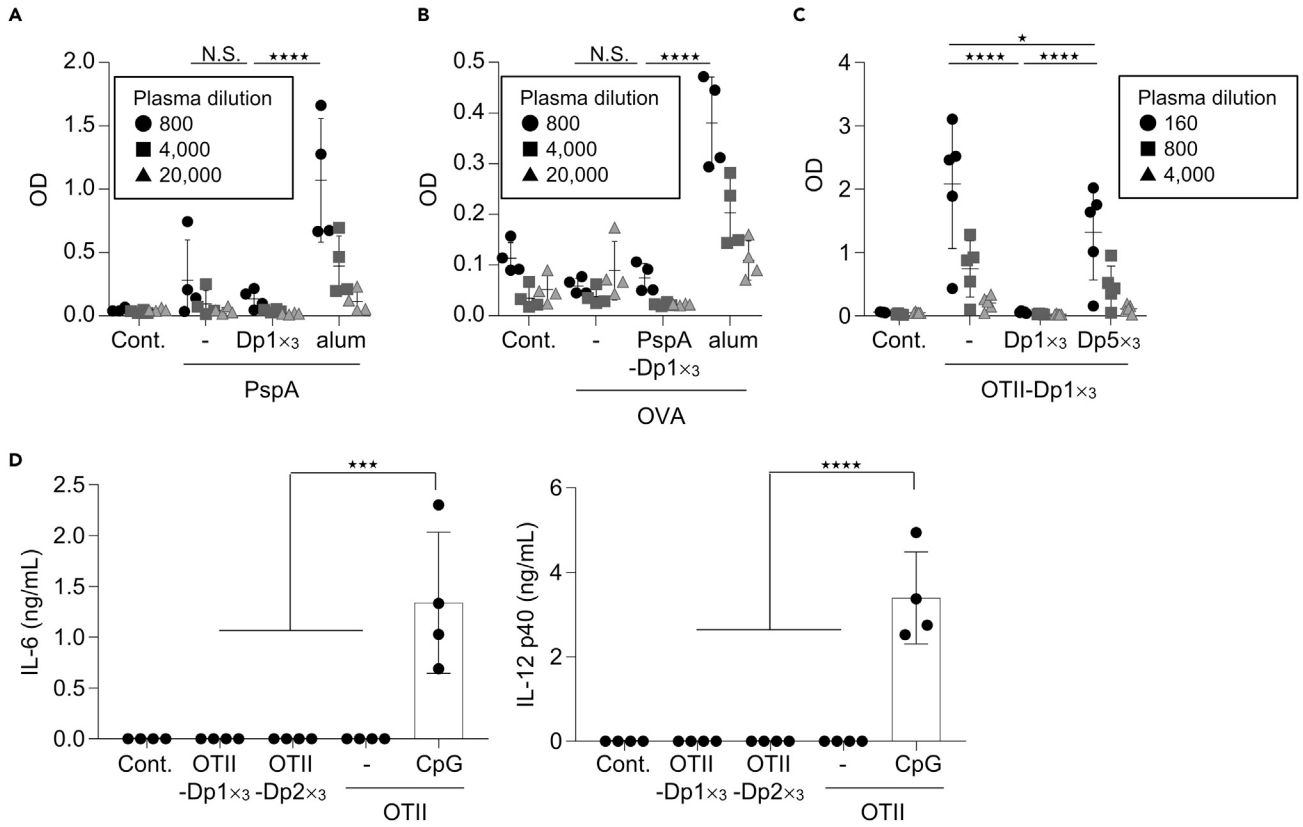

Figure 5. Importance of Dp1 and antigen fusion without DC activation

(A) Mice were immunized with 1 μg PspA alone, a mixture of 1 μg PspA and 1 μg free Dp1×3, or 1 μg PspA plus 250 μg alum, and the level of PspA-specific IgG in the plasma samples was evaluated at 7 days after the second immunization using ELISA.

(B) Mice were immunized with 10 μg OVA alone, 10 μg OVA plus 1 μg PspA-Dp1×3, or 10 μg OVA plus 250 μg alum, and the level of OVA-specific IgG in the plasma samples was evaluated 7 days after the second immunization using ELISA.

(C) Mice were immunized with 1.1 nmol (equivalent to 5 μg) OTII-Dp1×3, 1.1 nmol (equivalent to 5 μg) OTII-Dp1×3 plus 4 nmol (equivalent to 100 μg) free Dp1×3, or 1.1 nmol (equivalent to 5 μg) OTII-Dp1×3 plus 4 nmol (equivalent to 100 μg) free Dp5×3, and the level of OVA-specific IgG in the plasma samples was evaluated at 7 days after the second immunization using ELISA. (A–C) We used (A and B) 800- (●), 4,000- (■), and 20,000- (▲) fold–diluted, and (C) 160- (●), 800- (■), and 4,000- (▲) fold–diluted plasma samples.

(D) BMDCs were treated with 11.3 nM (equivalent to 50.9 μg/mL) OTII-Dp1×3, 11.3 nM (equivalent to 46.3 μg/mL) OTII-Dp2×3, 11.3 nM (equivalent to 20 μg/mL) OTII, or 11.3 nM (equivalent to 20 μg/mL) OTII plus 10 μg/mL CpG ODN for 24 h, and the levels of IL-6 and IL-12 p40 in the supernatants were determined using ELISA. (A and B) $n = 4$; (C) $n = 5$; (D) $n = 4$. Data are means ± SD. *$p < 0.05$, ***$p < 0.001$, ****$p < 0.0001$ as indicated by Tukey's test. N.S.: not significant. Significant differences were analyzed only in the (A and B) 800-fold-diluted and (C) 160-fold-diluted plasma samples.

free Dp1×3 or OTII-Dp1×3 plus free Dp5×3. Co-administration of OTII-Dp1×3 with free Dp1×3 inhibited OTII-Dp1×3-induced OVA-specific IgG response, whereas co-administration of free Dp5×3 did not inhibit OTII-Dp1×3-induced OVA-specific IgG response (Figure 5C). These results indicated that the binding receptor of Dp1 differs from that of other peptides. Furthermore, to examine whether Dp1 induces the activation of innate immune responses in DCs, BMDCs were treated with OTII-Dp1×3, OTII-Dp2×3, or CpG ODN *in vitro* (Figure 5D). Treatment with OTII-Dp1×3 and OTII-Dp2×3 did not induce the production of IL-6 and IL-12 p40, whereas OTII plus CpG ODN stimulated the production of IL-6 and IL-12 p40 (Figure 5D). Overall, these data suggest that the delivery of the antigen by Dp1 to immune cells such as DCs without stimulating the innate immune response might be important for the induction of antigen-specific antibody responses.

Efficient distribution of Dp1 to APCs

To further elucidate the mechanism of Dp1-induced immune responses, we examined the distribution of Dp1 in APCs, including DCs. To achieve this, mice were treated with fluorescent-labeled Dp1×3 or Dp2×3, and fluorescence-positive cells in draining lymph nodes was assessed 24 h after treatment using

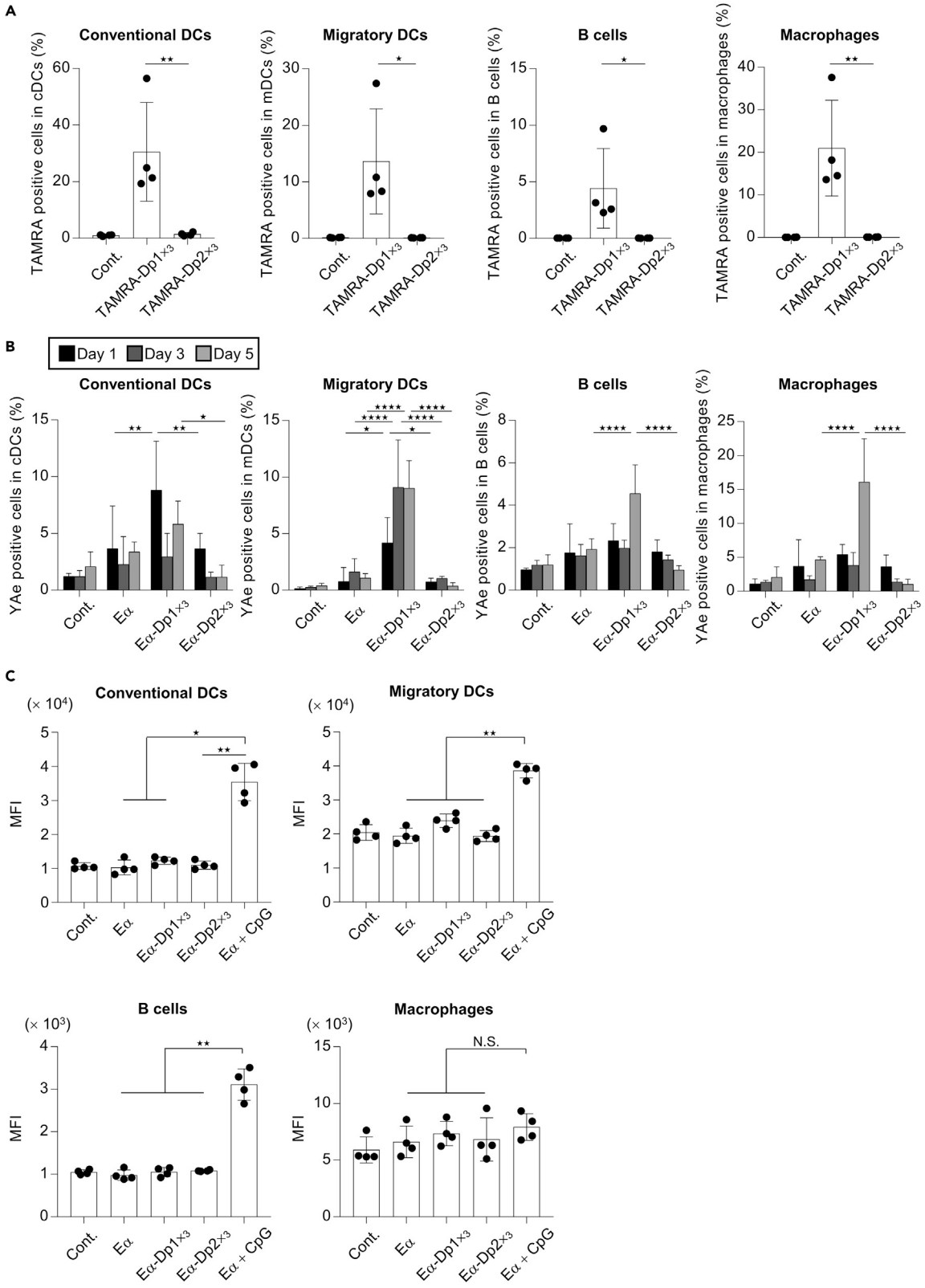
A
Conventional DCs
TAMRA positive cells in cDCs (%)
Migratory DCs
TAMRA positive cells in mDCs (%)
B cells
TAMRA positive cells in B cells (%)
Macrophages
TAMRA positive cells in macrophages (%)
Cont.
TAMRA-Dp1×3
TAMRA-Dp2×3
B
Day 1
Day 3
Day 5
YAe positive cells in cDCs (%)
YAe positive cells in mDCs (%)
YAe positive cells in B cells (%)
YAe positive cells in macrophages (%)
Eα
Eα-Dp1×3
Eα-Dp2×3
C
(× 10⁴)
MFI
Eα + CpG
(× 10³)
N.S.

Figure 6. Efficient antigen-presentation by Dp1 in mice

(A) Mice were treated with 3.5 nmol (equivalent to 10 μg) fluorescent-labeled Dp1×3 or 3.5 nmol (equivalent to 8.6 μg) fluorescent-labeled Dp2×3 via the ear pinna. Fluorescent-positive conventional DCs (cDCs), migratory DCs (mDCs), B cells, and macrophages in draining lymph nodes were measured 24 h after treatment using flow cytometry.

(B and C) Mice were treated with 18 nmol (equivalent to 30 μg) Eα only, 18 nmol (equivalent to 79 μg) Eα-Dp1×3, 18 nmol (equivalent to 72 μg) Eα-Dp2×3, or 18 nmol (equivalent to 30 μg) Eα plus 50 μg CpG ODN via the ear pinna.

(B) The presence of YAe positive cDCs, mDCs, B cells, and macrophages in draining lymph nodes was examined 1, 3, and 5 days after treatment using flow cytometry.

(C) The expression of CD86 on cDCs, mDCs, B cells, and macrophages was evaluated 3 day after treatment using flow cytometry.

(A–C) $n = 4$. Data are presented as means ± SD. *p< 0.05, **p< 0.01, ****p< 0.0001 as indicated by Tukey's test. N.S.: not significant. See also Figure S4.

flow cytometry. We observed significantly higher fluorescence-positive conventional DCs (cDCs), migratory DCs (mDCs), B cells, and macrophages in Dp1×3-treated mice than in Dp2×3-treated mice (Figures 6A, S4A, and S4B), indicating that there was efficient translocation of Dp1 into APCs. Furthermore, we examined the efficiency of antigen presentation on DCs using Eα peptide, which is an MHC class II epitope peptide (Itano et al., 2003). The Eα peptide present on MHC class II molecules was detected using flow cytometry using an antibody that recognizes the Eα peptide in complex with MHC class II (Itano et al., 2003). Eα-Dp1×3 fusion was synthesized chemically, and mice were treated with Eα, Eα-Dp1×3, or Eα-Dp2×3. At 1, 3, and 5 days after treatment, we detected antigen presentation on DCs, B cells, and macrophages in draining lymph nodes using flow cytometry (Figures 6B, S4A, and S4C). Furthermore, antigen presentation on cDCs was significantly higher in Eα-Dp1×3–treated mice than in Eα-treated and Eα-Dp2×3–treated mice on day 1 (Figures 6B, S4A, and S4C). In addition, Eα-Dp1×3 induced significantly higher antigen presentation on mDCs than Eα-Dp2×3 1, 3, and 5 days after treatment (Figures 6B, S4A, and S4C). Moreover, antigen presentation was significantly higher on B cells and macrophages in Eα-Dp1×3–treated mice on day 5 (Figure 6B). Furthermore, we did not observe enhanced expression of CD86, which is a co-stimulatory molecule, on DCs, B cells, and macrophages in Eα–, Eα-Dp1×3–, and Eα-Dp2×3–treated mice, whereas CpG ODN induced the enhanced expression of CD86 on DCs and B cells (Figure 6C). Collectively, these results suggest that Dp1 delivers antigens to APCs, such as DCs, B cells, and macrophages, and induces efficient antigen presentation without DC activation.

Binding of Dp1 to DCs in nucleolin-dependent manner

To understand how Dp1 delivers antigens to DCs, it is important to clarify the binding molecule of Dp1 on the surface of DCs. Because studies have shown that peptides with the R/K-X-X-R motif can bind to the ligand-binding pocket of neuropilin (NRP)-1 (Ruoslahti, 2017; Teesalu et al., 2009), we examined the binding of DC-targeting peptides to recombinant NRP-1 protein. DC-targeting peptides with R/K-X-X-R motif, including Dp1, could bind to the recombinant NRP-1 protein with similar affinity (Figure 7A). To examine the binding ability of these peptides to NRP-1 on the surface of mouse DCs, we examined the binding of these peptides to DC2.4 cells, a mouse DC line, in the presence of an anti-NRP-1 polyclonal antibody. The results showed that the binding of Dp2, Dp3, Dp4, and Dp5 to DC2.4 cells was significantly inhibited by the addition of anti-NRP-1 antibody compared with the isotype control antibody (Figure 7B). In contrast, there was no difference in Dp1-binding to anti-NRP-1 antibody-treated and isotype antibody-treated DC2.4 cells (Figure 7B). We also obtained similar results using different concentrations of anti-NRP-1 antibody and peptides (Figure S5). The binding of RPARPAR peptide, which is known to bind to NRP-1 (Teesalu et al., 2009), to DC2.4 cells was also significantly inhibited by the addition of anti-NRP-1 antibody compared with the isotype control antibody (Figure S5). To further verify the NRP-1-independent binding of Dp1 to DC2.4 cells, we suppressed the expression of NRP-1 in DC2.4 cells using anti-NRP-1 siRNA. We confirmed that the expression of NRP-1 in siRNA-transfected DC2.4 cells was significantly lower than that in wild-type DC2.4 cells (Figure S6A). No difference was found in Dp1-binding between wild-type DC2.4 cells and siRNA-transfected DC2.4 cells whereas the binding of Dp2, Dp4, Dp5, and RPARPAR peptide to siRNA-transfected DC2.4 cells was significantly lower than that in wild-type DC2.4 cells (Figures 7C and S6B). Collectively, these results suggest that Dp1 binding to DCs is independent of NRP-1.

To identify the cell receptor of Dp1 on DCs, the membrane fraction of BMDCs was incubated with Dp1-conjugated beads, and the bead-bound proteins were eluted using an acid solution. A Lumitein-stained gel after SDS-PAGE revealed a specific protein band (indicated with an arrow) with the sample from the Dp1-conjugated beads, whereas this band was not observed for the sample from the Dp5-conjugated beads (Figure 7D). Proteomic analysis of this band identified the protein as a nucleolin. To confirm the presence of nucleolin on the surface of DCs using flow cytometry, we used AS1411, a DNA aptamer specific for

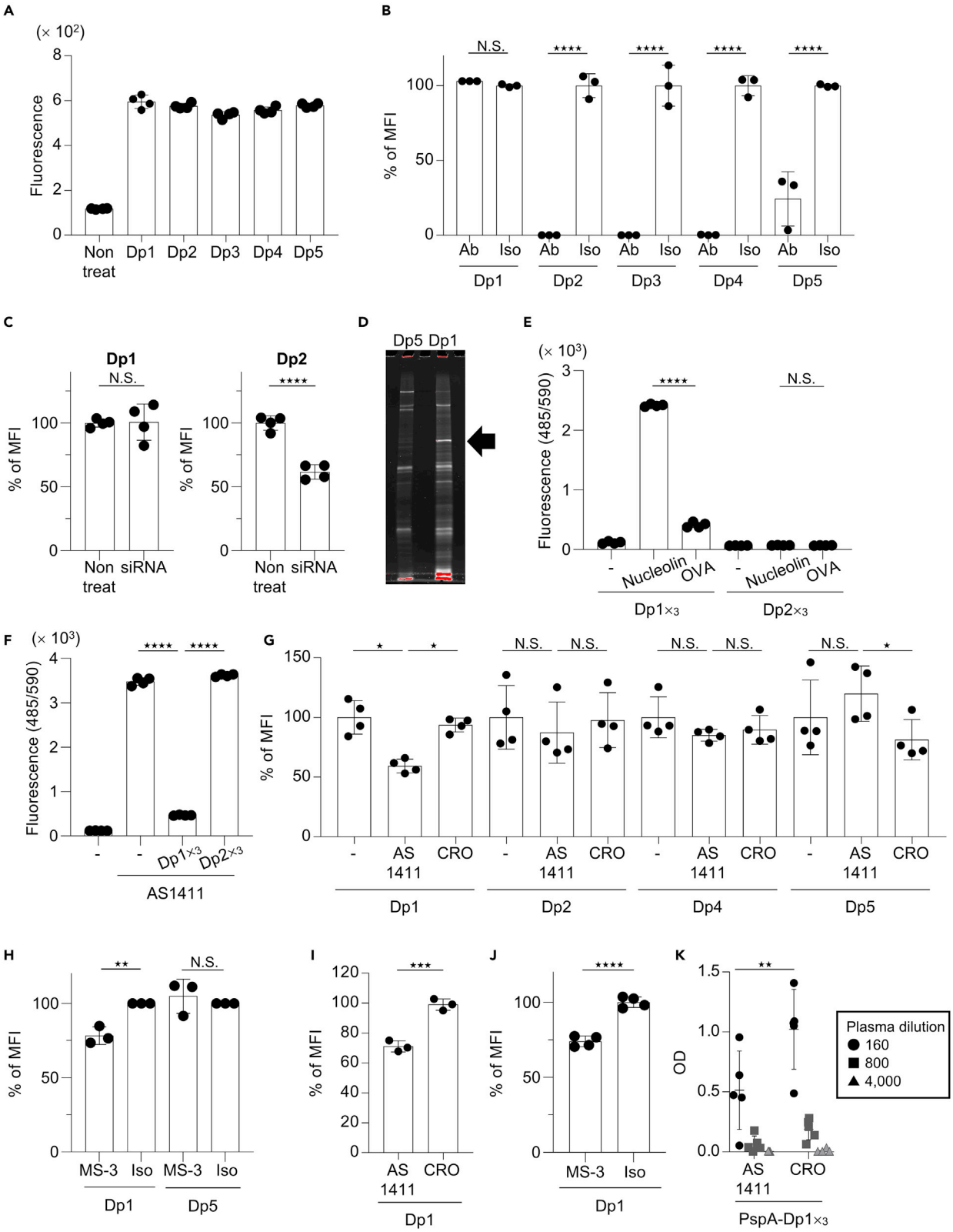
A
(× 10²)
Fluorescence
Non treat
Dp1
Dp2
Dp3
Dp4
Dp5
B
% of MFI
N.S.
****
Ab
Iso
Dp1
Dp2
Dp3
Dp4
Dp5
C
Dp1
Dp2
N.S.
****
% of MFI
Non treat
siRNA
D
Dp5 Dp1
E
(× 10³)
Fluorescence (485/590)
Nucleolin
OVA
Dp1×3
Dp2×3
F
(× 10³)
Fluorescence (485/590)
AS1411
G
% of MFI
AS 1411
CRO
H
MS-3
Iso
I
AS 1411
CRO
J
MS-3
Iso
K
OD
Plasma dilution
160
800
4,000
PspA-Dp1×3

Figure 7. Nucleolin as the cell surface receptor for Dp1

(A) The binding of 10 μg/mL biotin-labeled DC-targeting peptides to NRP-1 protein was detected using fluorescent-labeled streptavidin.

(B) The binding of each 250 μg/mL biotin-labeled DC-targeting peptide to DC2.4 cells in the presence of 90 μg/mL anti-NRP-1 polyclonal antibody or 90 μg/mL isotype control antibody was detected using flow cytometry using fluorescent-labeled streptavidin.

(C) The binding of 10 μg/mL biotin-labeled Dp1 or Dp2 to wild-type DC2.4 cells or DC2.4 cells treated with siRNA against NRP-1 were detected using flow cytometry using fluorescent-labeled streptavidin.

(D) The membrane fraction of BMDCs was incubated with Dp5-conjugated beads or Dp1-conjugated beads. The bead-bound proteins were eluted using an acid solution and the eluted solution was analyzed using Lumitein staining gel after SDS-PAGE. The arrow indicates the band of nucleolin.

(E) The binding of 10 μg/mL biotin-labeled Dp1×3 or Dp2×3 to recombinant nucleolin or OVA was measured using PE-labeled streptavidin.

(F) The binding of 0.5 μM biotin-labeled AS1411 to recombinant nucleolin in the presence or absence of 100 μg/mL Dp1×3 or Dp2×3 were measured using PE-labeled streptavidin.

(G) The binding of 10 μg/mL biotin-labeled Dp1, Dp2, Dp4, or Dp5 to DC2.4 cells in the presence of 10 μM AS1411 or CRO was detected using flow cytometry using fluorescent-labeled streptavidin.

(H) Flow cytometry was used to detect the binding of 10 μg/mL biotin-labeled Dp1 or Dp5 to DC2.4 cells in the presence of 50 μg/mL MS-3 or isotype control antibody using fluorescent-labeled streptavidin.

(I) The binding of 50 μg/mL biotin-labeled Dp1 to human CAL-1 cells in the presence of 10 μM AS1411 or CRO was evaluated using flow cytometry using fluorescent-labeled streptavidin.

(J) The binding of 50 μg/mL biotin-labeled Dp1 to human CAL-1 cells in the presence of 50 μg/mL MS-3 or isotype control antibody was detected using flow cytometry using fluorescent-labeled streptavidin.

(K) Mice were immunized with 1 μg PspA-Dp1×3 plus 5 nmol AS1411 or CRO, and the level of PspA-specific IgG in plasma was determined 20 days after the first immunization using ELISA. (A, C, E–G, and J) $n = 4$; (B, H, and I) $n = 3$; (K) $n = 5$. Data are means ± SD. *p< 0.05, **p< 0.01, ***p< 0.001, ****p< 0.0001 as indicated by (B, C, and H–K) Student's *t*-test and (E–G) Tukey's test. N.S.: not significant.

nucleolin, and a control oligonucleotide (CRO). AS1411 binds to DC2.4 cells (Figure S7A) and BMDCs (Figure S7B) at 4°C, whereas CRO did not bind to these DCs (Figures S7A and S7B), indicating the presence of nucleolin on the cell surface of DCs. Next, we measured the direct binding of biotin-labeled Dp1×3 to recombinant nucleolin protein using fluorescent-labeled streptavidin. Compared to the negative control protein OVA, biotin-labeled Dp1×3 bound significantly to recombinant nucleolin protein, whereas Dp2×3 failed to bind to recombinant nucleolin protein (Figure 7E). In addition, we examined whether Dp1×3 inhibited the binding of biotin-labeled AS1411 to recombinant nucleolin protein. Dp1×3 significantly suppressed the binding of AS1411 to recombinant nucleolin protein compared with Dp2×3 (Figure 7F). These results suggest that Dp1 binds to the nucleolin protein.

To assess the binding of Dp1 to nucleolin on DCs, we examined the binding of Dp1 to DC2.4 cells in the presence of AS1411 or CRO (Figure 7G). The binding of Dp1 to DC2.4 cells was significantly lower in the presence of AS1411 than in the presence of CRO; however, AS1411 did not inhibit the binding of Dp2, Dp4, and Dp5 to DC2.4 cells (Figure 7G). Next, we examined the binding of Dp1 to DC2.4 cells in the presence of MS-3, a monoclonal antibody specific to nucleolin. The binding of Dp1 to DC2.4 cells was significantly lower in the presence of MS-3 than in the presence of isotype control antibody; however, MS-3 did not inhibit the binding of Dp5 to DC2.4 cells (Figure 7H). In addition, AS1411 (Figure 7I) and MS-3 (Figure 7J) inhibited the binding of Dp1 to CAL-1 cells, which is a human DC line. Finally, to examine the contribution of nucleolin to Dp1-induced IgG response *in vivo*, mice were immunized with PspA-Dp1×3 in the presence of AS1411 or CRO. The level of PspA-specific IgG was significantly lower in PspA-Dp1×3 plus AS1411-immunized mice than in PspA-Dp1×3 plus CRO-immunized mice (Figure 7K). Collectively, these results suggest that nucleolin on the cell surface of DCs acts as the target molecule of Dp1.

DISCUSSION

In the present study, we successfully identified DC-targeting peptides using a phage display system. Most of the identified DC-targeting peptides had the R/K-X-X-R motif at the C-terminus (Figure 1K), indicating that the R/K-X-X-R motif is important for binding to DCs. Each phage clone had a strong binding ability to DCs (Figure 1B); however, only some of the synthetic peptides with the R/K-X-X-R motif could bind to DCs (Figures 1C and 1D). This discrepancy might result from the difference in sensitivity, as each phage displays 415 peptides on its surface (Teesalu et al., 2012) whereas synthetic peptides function as monomers. Among DC-targeting peptides with the R/K-X-X-R motif, Dp1 induced protein antigen-specific IgG even in the absence of adjuvant, which was comparable to the antigen (neutravidin and PspA) plus adjuvant induced response (Figures 1 and 2). Generally, it is difficult to induce peptide antigen-specific IgG, because peptide antigens have low antigenicity. Therefore, chemical conjugation of peptide antigens to carrier proteins, such as keyhole limpet hemocyanin, has been used to induce peptide antigen-specific IgG (Nakagami and Morishita, 2018). Here, we did not observe any OVA-specific IgG even in OTII plus adjuvant-immunized

mice (Figure 2G). In contrast, OTII-Dp1×3 induced strong OVA-specific IgG, even in the absence of adjuvants (Figures 2G and 2H). Therefore, Dp1 could be a useful carrier for not only protein antigens but also peptide antigens to improve antigen-specific antibody responses even in the absence of adjuvants.

Here, we showed that the combined use of Dp1 and CpG ODN improved the induction of antigen-specific IgG, especially IgG2, and antigen-specific IFN-γ producing $CD4^+$T cells (Figure 3). Mouse IgG2 corresponded to human IgG1 and IgG3. Mouse IgG2 and human IgG1 and IgG3 can bind to activating Fcγ receptors and induce strong antibody-dependent cellular cytotoxicity (ADCC) and antibody-dependent cellular phagocytosis (ADCP) by neutrophils and macrophages (Bournazos et al., 2017; Bruhns et al., 2009). ADCC and ADCP are important for eliminating bacteria including *S. pneumoniae* and virus-infected cells (Bournazos and Ravetch, 2015; Sadarangani, 2018). In addition, IFN-γ contributes to the elimination of pathogens by activating macrophages and neutrophils (Gocher et al., 2021; Sun et al., 2007). A recent study showed that both influenza virus-specific IgG2 and influenza virus-specific IFN-γ producing Th1 cells cooperatively confer protection against influenza virus infection in mice (Shibuya et al., 2021). Therefore, the combined use of antigens with Dp1 and CpG ODN could be a potential strategy for developing vaccines against bacteria such as *S. pneumoniae* and viruses such as influenza virus. Moreover, the findings of the present study showed that the combined use of Dp1 and CpG ODN induced long-lasting antigen-specific antibody response (Figure 3B). Long-lasting antibody responses are important to sustain long-term vaccine effects, and the decrease in antigen-specific IgG levels in blood indicates the need for a booster vaccination (Bemark et al., 2011; Wong and Bhattacharya, 2019). Therefore, this finding further validates the combined use of Dp1 and CpG ODN.

To elucidate why Dp1 alone can induce strong antibody response among DC-targeting peptides, we identified the binding receptor of DC-targeting peptides on DCs. Ruoslahti et al. found that peptides with the R/K-X-X-R/K motif at the C-terminus have the potential to bind to NRP-1 (Ruoslahti, 2017; Teesalu et al., 2009). In addition, studies have shown the usefulness of peptides with this motif as tumor tissue targeting vehicles (Ruoslahti, 2017; Teesalu et al., 2009). The findings of the present study showed that DC-targeting peptides with R/K-X-X-R motif, including Dp1, bind to recombinant NRP-1 protein, and the peptides except Dp1 bind to DCs in an NRP-1-dependent manner (Figures 7A–7C). In contrast, the binding of Dp1 to DCs is not dependent on NRP-1 (Figures 7A–7C). In addition, we showed the possibility that the binding receptor of Dp1 differs from that of other peptides (Figure 5C). We identified nucleolin as the cell surface receptor for Dp1 on DCs (Figures 7D–7J). Nucleolin is a major constituent of the nucleolus and is ubiquitously expressed in eukaryotic cells (Bates et al., 2017; Berger et al., 2015; Ferrara et al., 2021). Nucleolin plays crucial roles in the nucleus and cytoplasm by interacting with RNA, DNA, and other proteins (Bates et al., 2017; Berger et al., 2015; Ferrara et al., 2021). In addition, nucleolin is localized on the cell surface by interacting with other cell surface proteins in specific cell types, such as cancer and epithelial cells (Bates et al., 2017; Berger et al., 2015; Ferrara et al., 2021), although nucleolin does not have a transmembrane domain. Nucleolin located on the cell surface plays a critical role in the cell cycle and cell proliferation (Bates et al., 2017; Berger et al., 2015; Ferrara et al., 2021). Furthermore, nucleolin on the cell surface acts as a receptor for several types of growth factors, such as hepatocyte growth factor and viruses, including human respiratory syncytial virus. In addition, it participates in the translocation of several molecules and viruses from the cell surface into the cells (Bates et al., 2017; Berger et al., 2015; Ferrara et al., 2021). These findings indicate that extracellular ligands for nucleolin located on the cell surface can be internalized into cells after binding to nucleolin. For instance, AS1411, which is a DNA aptamer with high affinity and specificity to nucleolin, is the first tested aptamer in clinics for cancer therapy and has been used as a targeting carrier to deliver anti-cancer drugs to cancer cells (Bates et al., 2017; Li et al., 2017). The results of the present study showed that nucleolin is located on the cell surface of DCs; it plays a crucial role in the binding of Dp1 to DCs *in vitro* (Figures 7D–7J). Furthermore, we found that nucleolin contributes to antibody responses induced by Dp1 *in vivo* (Figure 7K). In addition, Dp1 efficiently delivered fusion antigens to DCs and induced efficient antigen presentation via MHC class II by DCs (Figures 6A and 6B). Therefore, efficient delivery of antigens by Dp1 to DCs via nucleolin following efficient antigen presentation on DCs contributes to strong antigen-specific antibody responses. Furthermore, the present study confirms the importance of the number of Dp1 to fuse with antigens and C-terminal exposure of Dp1 to improve immune responses (Figure 4). These structures might affect the binding affinity of Dp1 to nucleolin. Future investigation is needed to elucidate how Dp1 binds to nucleolin and what protein interacts with nucleolin on the cell surface of DCs. The physiological function of DC surface nucleolin must also be clarified. In addition, it is essential to clarify why the targeting of the antigen to nucleolin, not NRP-1,

induces antibody responses efficiently. Overall, these results suggest a vaccine strategy to deliver antigens to nucleolin by Dp1 or other vehicles to improve antigen-specific antibody responses. For instance, AS1411 might also be a useful antigen-delivery carrier to DCs and AS1411 conjugated antigens and adjuvants might be a safe vaccine.

The maturation status of DCs is important for regulating particular immune responses or promoting immunological unresponsiveness (i.e., tolerance) (Bonifaz et al., 2002; Chiang et al., 2019). For example, the activation of DCs is generally essential to induce antigen-specific immune responses. Adjuvants are generally necessary to induce antibody responses when proteins and peptides are used as antigens, because adjuvants induce DC activation (Del Giudice et al., 2018). In contrast to conventional adjuvants, Dp1 did not induce DC activation, such as cytokine production (Figures 5D and 6C). Thus, it remains unclear why efficient delivery of antigens by Dp1 without DC activation can induce efficient antibody responses. Although much of the focus in vaccine development is on the choice of antigen and adjuvant, another important parameter is the kinetics of antigen availability (Cirelli and Crotty, 2017; Irvine et al., 2020; Lofano et al., 2020). The findings of the present study showed that Dp1 induced a stronger and long-lasting antigen presentation on DCs (Figure 6B). For example, mDCs presented antigens for 5 days after treatment in Dp1-immunized mice (Figure 6B). Recent studies have provided evidence that slow release of antigens following antigen exposure in draining lymph nodes over periods of at least several days enhances the differentiation of follicular helper T cells (Baumjohann et al., 2013; Benson et al., 2015), which play important roles in the maturation of antigen-specific B cells, stimulate potent germinal center responses, and improve the quantity and quality of the antibodies (Cirelli et al., 2019; Pauthner et al., 2017; Tam et al., 2016). For instance, one of mechanisms for the adjuvanticity of alum has been believed to be an enhancement of antigen persistence and prolonged release, an effect referred to as the "depot effect" (Moyer et al., 2020). Therefore, longer antigen presentation of DCs by Dp1 might contribute to efficient antibody responses, and further investigation is needed.

Limitations of the study

For efficient translation of the results obtained in mice for human treatment, it is important to understand the differences in immune responses between mice and humans. Therefore, the findings of the present study confirm that Dp1 can deliver antigens to mouse and human DCs via nucleolin. However, the expression level and the expression pattern of nucleolin on several types of DCs between mice and humans might be different. Further studies are needed to translate our concept to human use in the future.

STAR★METHODS

Detailed methods are provided in the online version of this paper and include the following:

- KEY RESOURCES TABLE
- RESOURCE AVAILABILITY
  - Lead contact
  - Materials availability
  - Data and code availability
- EXPERIMENTAL MODEL AND SUBJECT DETAILS
  - Mice
- METHOD DETAILS
  - Peptides and proteins
  - Cells
  - Selection of DC-targeting peptides using phage library
  - Analysis of phage binding to DCs using flow cytometry
  - Binding assay using flow cytometry
  - Complex of neutravidin and DC-targeting peptide
  - Expression and purification of recombinant PspA proteins
  - Fusion of OTII or Eα with DC-targeting peptide
  - Immunization
  - *Streptococcus pneumoniae* challenge
  - Stimulation of BMDCs
  - Biodistribution of Dp1 *in vivo*
  - Antigen presentation on APCs *in vivo*

- Binding of DC-targeting peptides to NRP-1 protein
- Suppression of NRP1 expression using siRNA
- Recombinant nucleolin protein
- Binding of peptides and AS1411 to recombinant nucleolin protein
- Affinity chromatography
- Expression level of cell-surface nucleolin on DCs

- QUANTIFICATION AND STATISTICAL ANALYSIS
  - Statistical analyses

SUPPLEMENTAL INFORMATION

Supplemental information can be found online at https://doi.org/10.1016/j.isci.2022.105324.

ACKNOWLEDGMENTS

This study was supported by grants from the Japan Society for the Promotion of Science (JSPS KAKENHI Grant Numbers JP17H04009, JP18K19401, JP20K21480, and JP20H03404 to Y.Y.), Japan Agency for Medical Research and Development (AMED: Research Program on Emerging and Re-emerging Infectious Diseases grant (grant number JP20fk0108074) to Y.Y.), BIKEN Taniguchi Scholarship (to T.M.), and Nagai Memorial Research Scholarship from the Pharmaceutical Society of Japan (to S. Tamiya).

AUTHOR CONTRIBUTIONS

T.M., K.M., S. Tamiya, and Y.Y. designed the experiments. T.M., K.M., S. Tamiya, S. Takahama performed the experiments. T.M., K.M., S. Tamiya, and Y.Y. performed the data analysis and interpretation. Y.A., I.N., E.K., M.N., T.Y., and M.N.F. supported the experimental design and edited the manuscript. T.M. and Y.Y. wrote the manuscript. Y.Y. oversaw the study. All authors have read and agreed to the published version of the manuscript.

DECLARATION OF INTERESTS

Yasuo Yoshioka has patent DENDRITIC-CELL-TARGETED PEPTIDE, FUSION PEPTIDE UTILIZING SAID PEPTIDE, AND VACCINE UTILIZING SAID FUSION PEPTIDE (US 11,186,618) to The Research Foundation for Microbial Diseases of Osaka University. Yasuo Yoshioka is an employee of the Research Foundation for Microbial Diseases of Osaka University. The other authors declare no conflicts of interest.

Received: May 26, 2022
Revised: August 28, 2022
Accepted: October 6, 2022
Published: November 18, 2022

REFERENCES

Bates, P.J., Reyes-Reyes, E.M., Malik, M.T., Murphy, E.M., O'Toole, M.G., and Trent, J.O. (2017). G-quadruplex oligonucleotide AS1411 as a cancer-targeting agent: uses and mechanisms. Biochim. Biophys. Acta Gen. Subj. *1861*, 1414–1428.

Baumjohann, D., Preite, S., Reboldi, A., Ronchi, F., Ansel, K.M., Lanzavecchia, A., and Sallusto, F. (2013). Persistent antigen and germinal center B cells sustain T follicular helper cell responses and phenotype. Immunity *38*, 596–605.

Beerli, R.R., and Rader, C. (2010). Mining human antibody repertoires. mAbs *2*, 365–378.

Bemark, M., Bergqvist, P., Stensson, A., Holmberg, A., Mattsson, J., and Lycke, N.Y. (2011). A unique role of the cholera toxin A1-DD adjuvant for long-term plasma and memory B cell development. J. Immunol. *186*, 1399–1410.

Benson, R.A., MacLeod, M.K., Hale, B.G., Patakas, A., Garside, P., and Brewer, J.M. (2015). Antigen presentation kinetics control T cell/dendritic cell interactions and follicular helper T cell generation *in vivo*. Elife *4*, e06994.

Berger, C.M., Gaume, X., and Bouvet, P. (2015). The roles of nucleolin subcellular localization in cancer. Biochimie *113*, 78–85.

Bonifaz, L., Bonnyay, D., Mahnke, K., Rivera, M., Nussenzweig, M.C., and Steinman, R.M. (2002). Efficient targeting of protein antigen to the dendritic cell receptor DEC-205 in the steady state leads to antigen presentation on major histocompatibility complex class I products and peripheral CD8+ T cell tolerance. J. Exp. Med. *196*, 1627–1638.

Bournazos, S., and Ravetch, J.V. (2015). Fcgamma receptor pathways during active and passive immunization. Immunol. Rev. *268*, 88–103.

Bournazos, S., Wang, T.T., Dahan, R., Maamary, J., and Ravetch, J.V. (2017). Signaling by antibodies: recent progress. Annu. Rev. Immunol. *35*, 285–311.

Bruhns, P., Iannascoli, B., England, P., Mancardi, D.A., Fernandez, N., Jorieux, S., and Daëron, M. (2009). Specificity and affinity of human Fcgamma receptors and their polymorphic variants for human IgG subclasses. Blood *113*, 3716–3725.

Caminschi, I., and Shortman, K. (2012). Boosting antibody responses by targeting antigens to dendritic cells. Trends Immunol. *33*, 71–77.

Chiang, C.Y., Wu, C.C., Chen, Y.J., Liu, S.J., Leng, C.H., and Chen, H.W. (2019). Delivery of antigen to CD8(+) dendritic cells by fusing antigen with formyl peptide receptor-like 1 inhibitor protein induces antitumor immunity. Front. Immunol. *10*, 1839.

Cid, R., and Bolívar, J. (2021). Platforms for production of protein-based vaccines: from classical to next-generation strategies. Biomolecules *11*, 1072.

Cirelli, K.M., and Crotty, S. (2017). Germinal center enhancement by extended antigen availability. Curr. Opin. Immunol. *47*, 64–69.

Cirelli, K.M., Carnathan, D.G., Nogal, B., Martin, J.T., Rodriguez, O.L., Upadhyay, A.A., Enemuo, C.A., Gebru, E.H., Choe, Y., Viviano, F., et al. (2019). Slow delivery immunization enhances HIV neutralizing antibody and germinal center responses via modulation of immunodominance. Cell *177*, 1153–1171.e28.

Del Giudice, G., Rappuoli, R., and Didierlaurent, A.M. (2018). Correlates of adjuvanticity: a review on adjuvants in licensed vaccines. Semin. Immunol. *39*, 14–21.

Delany, I., Rappuoli, R., and De Gregorio, E. (2014). Vaccines for the 21st century. EMBO Mol. Med. *6*, 708–720.

Dhodapkar, M.V., Sznol, M., Zhao, B., Wang, D., Carvajal, R.D., Keohan, M.L., Chuang, E., Sanborn, R.E., Lutzky, J., Powderly, J., et al. (2014). Induction of antigen-specific immunity with a vaccine targeting NY-ESO-1 to the dendritic cell receptor DEC-205. Sci. Transl. Med. *6*, 232ra251.

Eisenbarth, S.C. (2019). Dendritic cell subsets in T cell programming: location dictates function. Nat. Rev. Immunol. *19*, 89–103.

Ferrara, B., Belbekhouche, S., Habert, D., Houppe, C., Vallée, B., Bourgoin-Voillard, S., Cohen, J.L., Cascone, I., and Courty, J. (2021). Cell surface nucleolin as active bait for nanomedicine in cancer therapy: a promising option. Nanotechnology *32*, 322001.

Fukuda, M.N., Ohyama, C., Lowitz, K., Matsuo, O., Pasqualini, R., Ruoslahti, E., and Fukuda, M. (2000). A peptide mimic of E-selectin ligand inhibits sialyl Lewis X-dependent lung colonization of tumor cells. Cancer Res. *60*, 450–456.

Gocher, A.M., Workman, C.J., and Vignali, D.A.A. (2021). Interferon-gamma: teammate or opponent in the tumour microenvironment? Nat. Rev. Immunol. *22*, 158–172.

Gou, S., Wang, S., Liu, W., Chen, G., Zhang, D., Du, J., Yan, Z., Wang, H., Zhai, W., Sui, X., et al. (2021). Adjuvant-free peptide vaccine targeting Clec9a on dendritic cells can induce robust antitumor immune response through Syk/IL-21 axis. Theranostics *11*, 7308–7321.

Goyvaerts, C., and Breckpot, K. (2015). Pros and cons of antigen-presenting cell targeted tumor vaccines. J. Immunol. Res. *2015*, 785634.

Graham, B.S., and Sullivan, N.J. (2018). Emerging viral diseases from a vaccinology perspective: preparing for the next pandemic. Nat. Immunol. *19*, 20–28.

Heikenwalder, M., Polymenidou, M., Junt, T., Sigurdson, C., Wagner, H., Akira, S., Zinkernagel, R., and Aguzzi, A. (2004). Lymphoid follicle destruction and immunosuppression after repeated CpG oligodeoxynucleotide administration. Nat. Med. *10*, 187–192.

HogenEsch, H., O'Hagan, D.T., and Fox, C.B. (2018). Optimizing the utilization of aluminum adjuvants in vaccines: you might just get what you want. NPJ Vaccines *3*, 51.

Hoogenboom, H.R., de Bruïne, A.P., Hufton, S.E., Hoet, R.M., Arends, J.W., and Roovers, R.C. (1998). Antibody phage display technology and its applications. Immunotechnology *4*, 1–20.

Hossain, M.K., and Wall, K.A. (2019). Use of dendritic cell receptors as targets for enhancing anti-cancer immune responses. Cancers *11*, 418.

Idoyaga, J., Lubkin, A., Fiorese, C., Lahoud, M.H., Caminschi, I., Huang, Y., Rodriguez, A., Clausen, B.E., Park, C.G., Trumpfheller, C., and Steinman, R.M. (2011). Comparable T helper 1 (Th1) and CD8 T-cell immunity by targeting HIV gag p24 to CD8 dendritic cells within antibodies to Langerin, DEC205, and Clec9A. Proc. Natl. Acad. Sci. USA *108*, 2384–2389.

Irvine, D.J., Aung, A., and Silva, M. (2020). Controlling timing and location in vaccines. Adv. Drug Deliv. Rev. *158*, 91–115.

Irvine, D.J., Swartz, M.A., and Szeto, G.L. (2013). Engineering synthetic vaccines using cues from natural immunity. Nat. Mater. *12*, 978–990.

Itano, A.A., McSorley, S.J., Reinhardt, R.L., Ehst, B.D., Ingulli, E., Rudensky, A.Y., and Jenkins, M.K. (2003). Distinct dendritic cell populations sequentially present antigen to CD4 T cells and stimulate different aspects of cell-mediated immunity. Immunity *19*, 47–57.

Khan, N., and Jan, A.T. (2017). Towards identifying protective B-cell epitopes: the PspA story. Front. Microbiol. *8*, 742.

Kobiyama, K., Saigusa, R., and Ley, K. (2019). Vaccination against atherosclerosis. Curr. Opin. Immunol. *59*, 15–24.

Krammer, F. (2019). The human antibody response to influenza A virus infection and vaccination. Nat. Rev. Immunol. *19*, 383–397.

Li, F., Lu, J., Liu, J., Liang, C., Wang, M., Wang, L., Li, D., Yao, H., Zhang, Q., Wen, J., et al. (2017). A water-soluble nucleolin aptamer-paclitaxel conjugate for tumor-specific targeting in ovarian cancer. Nat. Commun. *8*, 1390.

Lofano, G., Mallett, C.P., Bertholet, S., and O'Hagan, D.T. (2020). Technological approaches to streamline vaccination schedules, progressing towards single-dose vaccines. NPJ Vaccines *5*, 88.

Lonn, P., and Dowdy, S.F. (2015). Cationic PTD/CPP-mediated macromolecular delivery: charging into the cell. Expert Opin. Drug Deliv. *12*, 1627–1636.

Macri, C., Dumont, C., Johnston, A.P., and Mintern, J.D. (2016). Targeting dendritic cells: a promising strategy to improve vaccine effectiveness. Clin. Transl. Immunol. *5*, e66.

Maeda, T., Murata, K., Fukushima, T., Sugahara, K., Tsuruda, K., Anami, M., Onimaru, Y., Tsukasaki, K., Tomonaga, M., Moriuchi, R., et al. (2005). A novel plasmacytoid dendritic cell line, CAL-1, established from a patient with blastic natural killer cell lymphoma. Int. J. Hematol. *81*, 148–154.

Malonis, R.J., Lai, J.R., and Vergnolle, O. (2020). Peptide-based vaccines: current progress and future challenges. Chem. Rev. *120*, 3210–3229.

Mann, A.P., Scodeller, P., Hussain, S., Joo, J., Kwon, E., Braun, G.B., Mölder, T., She, Z.G., Kotamraju, V.R., Ranscht, B., et al. (2016). A peptide for targeted, systemic delivery of imaging and therapeutic compounds into acute brain injuries. Nat. Commun. *7*, 11980.

Masomian, M., Ahmad, Z., Gew, L.T., and Poh, C.L. (2020). Development of next generation Streptococcus pneumoniae vaccines conferring broad protection. Vaccines (Basel) *8*, 132.

Moyer, T.J., Kato, Y., Abraham, W., Chang, J.Y.H., Kulp, D.W., Watson, N., Turner, H.L., Menis, S., Abbott, R.K., Bhiman, J.N., et al. (2020). Engineered immunogen binding to alum adjuvant enhances humoral immunity. Nat. Med. *26*, 430–440.

Moyer, T.J., Zmolek, A.C., and Irvine, D.J. (2016). Beyond antigens and adjuvants: formulating future vaccines. J. Clin. Invest. *126*, 799–808.

Mukai, Y., Yoshioka, Y., and Tsutsumi, Y. (2005). Phage display and PEGylation of therapeutic proteins. Comb. Chem. High Throughput Screen. *8*, 145–152.

Nakagami, H., and Morishita, R. (2018). Therapeutic vaccines for hypertension: a new option for clinical practice. Curr. Hypertens. Rep. *20*, 22.

Pardi, N., Hogan, M.J., Porter, F.W., and Weissman, D. (2018). mRNA vaccines - a new era in vaccinology. Nat. Rev. Drug Discov. *17*, 261–279.

Pauthner, M., Havenar-Daughton, C., Sok, D., Nkolola, J.P., Bastidas, R., Boopathy, A.V., Carnathan, D.G., Chandrashekar, A., Cirelli, K.M., Cottrell, C.A., et al. (2017). Elicitation of robust tier 2 neutralizing antibody responses in nonhuman primates by HIV envelope trimer immunization using optimized approaches. Immunity *46*, 1073–1088.e6.

Plotkin, S.A. (2009). Vaccines: the fourth century. Clin. Vaccine Immunol. *16*, 1709–1719.

Ruoslahti, E. (2017). Tumor penetrating peptides for improved drug delivery. Adv. Drug Deliv. Rev. *110–111*, 3–12.

Sadarangani, M. (2018). Protection against invasive infections in children caused by encapsulated bacteria. Front. Immunol. *9*, 2674.

Saxena, M., van der Burg, S.H., Melief, C.J.M., and Bhardwaj, N. (2021). Therapeutic cancer vaccines. Nat. Rev. Cancer *21*, 360–378.

Scodeller, P., Simón-Gracia, L., Kopanchuk, S., Tobi, A., Kilk, K., Säälik, P., Kurm, K., Squadrito, M.L., Kotamraju, V.R., Rinken, A., et al. (2017). Precision targeting of tumor macrophages with a CD206 binding peptide. Sci. Rep. *7*, 14655.

Seya, T., Shime, H., Takeda, Y., Tatematsu, M., Takashima, K., and Matsumoto, M. (2015). Adjuvant for vaccine immunotherapy of cancer–focusing on Toll-like receptor 2 and 3 agonists for safely enhancing antitumor immunity. Cancer Sci. *106*, 1659–1668.

Shibuya, M., Tamiya, S., Kawai, A., Hirai, T., Cragg, M.S., and Yoshioka, Y. (2021). Synergistic effect of non-neutralizing antibodies and interferon-gamma for cross-protection against influenza. iScience *24*, 103131.

Shirota, H., and Klinman, D.M. (2014). Recent progress concerning CpG DNA and its use as a vaccine adjuvant. Expert Rev. Vaccines *13*, 299–312.

Sioud, M., Skorstad, G., Mobergslien, A., and Sæbøe-Larssen, S. (2013). A novel peptide carrier for efficient targeting of antigens and nucleic acids to dendritic cells. Faseb. J. *27*, 3272–3283.

Sugihara, K., Kobayashi, Y., Suzuki, A., Tamura, N., Motamedchaboki, K., Huang, C.T., Akama, T.O., Pecotte, J., Frost, P., Bauer, C., et al. (2014). Development of pro-apoptotic peptides as potential therapy for peritoneal endometriosis. Nat. Commun. *5*, 4478.

Sun, K., Salmon, S.L., Lotz, S.A., and Metzger, D.W. (2007). Interleukin-12 promotes gamma interferon-dependent neutrophil recruitment in the lung and improves protection against respiratory Streptococcus pneumoniae infection. Infect. Immun. *75*, 1196–1202.

Tacken, P.J., and Figdor, C.G. (2011). Targeted antigen delivery and activation of dendritic cells *in vivo*: steps towards cost effective vaccines. Semin. Immunol. *23*, 12–20.

Tam, H.H., Melo, M.B., Kang, M., Pelet, J.M., Ruda, V.M., Foley, M.H., Hu, J.K., Kumari, S., Crampton, J., Baldeon, A.D., et al. (2016). Sustained antigen availability during germinal center initiation enhances antibody responses to vaccination. Proc. Natl. Acad. Sci. USA *113*, E6639–E6648.

Teesalu, T., Sugahara, K.N., and Ruoslahti, E. (2012). Mapping of vascular ZIP codes by phage display. Methods Enzymol. *503*, 35–56.

Teesalu, T., Sugahara, K.N., Kotamraju, V.R., and Ruoslahti, E. (2009). C-end rule peptides mediate neuropilin-1-dependent cell, vascular, and tissue penetration. Proc. Natl. Acad. Sci. USA *106*, 16157–16162.

Trumpfheller, C., Longhi, M.P., Caskey, M., Idoyaga, J., Bozzacco, L., Keler, T., Schlesinger, S.J., and Steinman, R.M. (2012). Dendritic cell-targeted protein vaccines: a novel approach to induce T-cell immunity. J. Intern. Med. *271*, 183–192.

Wong, R., and Bhattacharya, D. (2019). Basics of memory B-cell responses: lessons from and for the real world. Immunology *156*, 120–129.

Yan, Z., Wu, Y., Du, J., Li, G., Wang, S., Cao, W., Zhou, X., Wu, C., Zhang, D., Jing, X., et al. (2016). A novel peptide targeting Clec9a on dendritic cell for cancer immunotherapy. Oncotarget *7*, 40437–40450.

STAR★METHODS

KEY RESOURCES TABLE

REAGENT or RESOURCE	SOURCE	IDENTIFIER
Antibodies		
Goat polyclonal anti-mouse IgG with HRP	Merck Millipore	Cat# AP503P RRID: AB_805355
Goat polyclonal anti-mouse IgG1 with HRP	SouthernBiotech	Cat# 1070-05; RRID: AB_2650509
Goat polyclonal anti-mouse IgG2c with HRP	SouthernBiotech	Cat# 1079-05; RRID: AB_2794466
Anti-mouse CD16/CD32 (clone: 93)	BioLegend	Cat# 101302; RRID: AB_312801
BV421 anti-mouse I-A/I-E (clone: M5/114.15.2)	BioLegend	Cat# 107632; RRID: AB_2650896
Alexa Fluor 700 anti-mouse CD19 (clone: 6D5)	BioLegend	Cat# 115528; RRID: AB_493735
APC anti-mouse PDCA1 (clone: 927)	BioLegend	Cat# 127016; RRID: AB_1967127
PerCP/Cy5.5 anti-mouse CD11c (clone: N418)	BioLegend	Cat# 117328; RRID: AB_2129641
BV421 anti-mouse CD304 (Neuropilin-1) (clone: 3E12)	BioLegend	Cat# 145209; RRID: AB_2562358
Anti-T7 tail fiber monoclonal antibody	Novagen	Cat# 71530
Biotin-labelled anti-mouse IgG2a antibody (clone: RMG2a-62)	BioLegend	Cat# 407104; RRID: AB_345324
Anti-NRP-1 polyclonal antibody	R&D Systems	Cat# AF566
Control antibody (NRP-1)	R&D Systems	Cat# AB-108-C
Anti-nucleolin monoclonal antibody	Santa Cruz	Cat# sc-8031
Control antibody (nucleolin) (clone: MOPC-21)	BioLegend	Cat# 400102; RRID: AB_2891079
Biotin-labelled Y-ae antibody	eBioscience	Cat# 13-5741-82; RRID: AB_657821
Bacterial and virus strains		
A T7 phage library displaying random 7-mer linear peptides	Dr. Erkki Ruoslahti, Sanford Burnham Prebys Medical Discovery Institute	N/A
Escherichia coli BL21	New England Biolabs,Inc.	Cat# C2527I
WU2 strain of *Streptococcus pneumoniae*	Dr. Yasuhiro Akeda, Research Institute for Microbial Diseases, Osaka University	N/A
Chemicals, peptides, and recombinant proteins		
Human Fms-related tyrosine kinase 3 ligand	Miltenyi Biotech	Cat# 130-093-854
Alhydrogel Adjuvant 2%	InvivoGen	Cat# vac-alu-250
Block Ace	DS Pharma Biomedical	Cat# UKB80
Tetramethyl Benzidine	Nacalai Tesque	Cat# 05299-54
2 N H_2SO_4	Nacalai Tesque	Cat# 95626-06
PE-labelled streptavidin	BioLegend	Cat# 405204
Peptides (Dp1 etc.)	Scrum	N/A
Biotin-labelled peptide	Scrum	N/A
TAMRA-labelled trimeric peptides	Scrum	N/A
OTII peptide (ISQAVHAAHAEINEAGR)	Scrum	N/A
OTII fusion with DC-targeting peptides	Scrum	N/A
Eα peptide (ASFEAQGALANIAVDKA)	Scrum	N/A
Eα fusion with DC-targeting peptides	Scrum	N/A
Neutravidin	Thermo Fisher Scientific	Cat# 31000
Ultrafiltration tubes (10 kDa)	Merck Millipore	Cat# UFC801024
Isopropyl-β-D-1-thiogalactopyranoside	Nacalai Tesque	Cat# 19742-94
Protease inhibitors	Roche	Cat# 11836170001
Ni-Sepharose HisTrap FF column	GE Healthcare	Cat# 17531901
Superose 6 Increase 10/300 GL column	GE Healthcare	Cat# 29091596

(*Continued on next page*)

Continued

REAGENT or RESOURCE	SOURCE	IDENTIFIER
EndoTrap® HD column	LIONEX	Cat# LET0010
Limulus Color KY Test	Wako Pure Chemical Industries	Cat# 291-53101
White OptiPlate-96	Perkin-Elmer	Cat# 6005290
OVA with low endotoxin content	Fujifilm	Cat# 011-24733
Grade V OVA	Sigma-Aldrich	Cat# A5503
Recombinant mouse NRP-1 protein	R&D Systems	Cat# 5994-N1
Lipofectamine 3000	Thermo Fisher Scientific	Cat# L3000008
HM-NeutrAvidin beads	Tamagawa Seiki	Cat# TAB8848N3171
Lumitein	Biotium	Cat# 21002
Deoxyribonuclease 1	Wako	Cat# 047-26771
Liberase TL	Roche Diagnostics GmbH	Cat# 5401020001
7-amino-actinomycin D (7-AAD)	BioLegend	Cat# 420404
Fixable Viability Dye eFluor 780	Thermo Fisher Scientific	Cat# 65-0865-14
Critical commercial assays		
IFN-γ ELISA Kit	BioLegend	Cat# 430801
IL-6 ELISA kit	BioLegend	Cat# 431301
IL-12 p40 ELISA kit	BioLegend	Cat# 431601
Pierce BCA Protein Assay Kit	Thermo Fisher Scientific	Cat# 23225
Experimental models: Cell lines		
EL4 cells	ATCC	N/A
B16-F10 cells	ATCC	N/A
DC2.4 cells	Dr. KL Rock, University of Massachusetts Medical School	N/A
CAL-1 cells	Dr. Takahiro Maeda, Nagasaki University	N/A
Experimental models: Organisms/strains		
C57BL/6JJmsSlc	Japan SLC	N/A
BALB/c	Japan SLC	N/A
Oligonucleotides		
CpG–ODN (CpG K3: 5′-atcgactctcgagcgttctc-3′)	Gene Design	Cat# CN-65003
AS1411(5′-tttggtggtggtggttgtggtggtggtgg-3′)	Hokkaido System Science	N/A
CRO (5′-tttcctcctcctccttctcctcctcctcct-3′)	Hokkaido System Science	N/A
siRNA NRP-1 (5′-ctgctacttcacagtatggta-3′)	Qiagen	N/A
pET28a vector	Merck Millipore	Cat# 69864
pGEX-6P-2 vector	Merck Millipore	Cat# 28-9546-50
Software and algorithms		
GraphPad Prism 7.03	GraphPad Software	Version 7.03
Flowjo Software	TreeStar	N/A
Other		
Microplate Reader (Power Wave HT)	BioTek	N/A
Multi-plate reader	DS Pharma Biomedical	N/A
NovoCyte Flow Cytometer	ACEA Bioscience	N/A
Attune NxT Flow Cytometer	Thermo Fisher Scientific	N/A
AKTA pure 25 L1	GE Healthcare	N/A

RESOURCE AVAILABILITY

Lead contact

Further information and requests for resources and reagents should be directed to, and will be fulfilled by, the Lead Contact, Yasuo Yoshioka (y-yoshioka@biken.osaka-u.ac.jp).

Materials availability

All reagents used in this study will be made available upon reasonable request to the lead contact.

Data and code availability

- All data reported in this paper will be shared by the lead contact upon request.
- This paper does not report original code.
- Any additional information required to reanalyze the data reported in this paper is available from the lead contact upon request.

EXPERIMENTAL MODEL AND SUBJECT DETAILS

Mice

Male C57BL/6J and BALB/c mice (6–7-week-old) were purchased from SLC (Hamamatsu, Japan). BALB/c mice were used only, as shown in Figure 2C. Mice were housed in a room under a 12-h:12-h light:dark cycle (lights on, 8:00 a.m.; lights off, 8:00 p.m.) and allowed unrestricted access to food and water. Animal experiments were conducted in accordance to Osaka University's Institutional Guidelines for the Ethical Treatment of Animals and was approved by the Animal Care and Use Committee of the Research Institute for Microbial Diseases, Osaka University, Japan (protocol number: BIKEN-AP-R01-15-1).

METHOD DETAILS

Peptides and proteins

All the peptides and proteins used in this study are listed in Table S1.

Cells

EL4 cells, a mouse T-cell lymphoma cell line, and B16-F10 cells, a mouse melanoma cell line, were obtained from the American Type Culture Collection (Manassas, VA, USA). EL4 cells and B16-F10 cells were cultured in DMEM supplemented with 10% fetal calf serum and 1% penicillin and streptomycin. DC2.4 cells, a mouse dendritic cell line, was kindly provided by Dr. KL Rock (Department of Pathology, University of Massachusetts Medical School, Worcester, MA, USA). DC2.4 cells were cultured in RPMI1640 supplemented with 10% fetal calf serum, 1% penicillin and streptomycin, 1% nonessential amino acids, 10 mM HEPES, and 2-mercaptoethanol. CAL-1 cells, a human pDC line isolated from a lymphoma patient, was kindly provided by Dr. Takahiro Maeda (Nagasaki University, Nagasaki, Japan) (Maeda et al., 2005). CAL-1 cells were cultured in RPMI1640 supplemented with 10% fetal calf serum, 1% penicillin and streptomycin, 1% nonessential amino acids, 10 mM HEPES, and 1 mM sodium pyruvate. To generate mouse-derived BMDCs, we isolated bone marrow cells from the femurs of C57BL/6J mice and cultured the cells at 37°C for 7 days in RPMI1640 supplemented with 10% fetal calf serum and 1% penicillin and streptomycin with 100 ng/mL human Fms-related tyrosine kinase 3 ligand (Miltenyi Biotech, Bergisch Gladbach, Germany). These cells were maintained at 37°C in a humidified incubator with 5% CO_2.

Selection of DC-targeting peptides using phage library

A T7 phage library displaying random 7-mer linear peptides was provided by Dr. E. Ruoslahti (Sanford Burnham Prebys Medical Discovery Institute, La Jolla, CA, USA.). Prior to mixing the phage library with mouse-derived BMDCs, the phage library with 3.6×10^9 plaque-forming units was mixed with EL4 cells (1×10^8 cells) in PBS containing 2% skim milk at 25°C for 1 h with gentle shaking. The cells were centrifuged at 1,300 rpm for 5 min, and the supernatant was recovered. The supernatant was incubated with B16-F10 cells (1×10^6 cells) cultured in 6-well plates containing PBS supplemented with 2% skim milk at 25°C for 1 h. The supernatant was recovered and the subtracted phage library was incubated with BMDCs (4×10^6 cells) cultured in 6-well plates containing PBS supplemented with 2% skim milk at 4°C for 1 h. BMDCs were washed with PBS and BMDC-associated phages were recovered by adding 1% NP-40 in PBS, and *Escherichia coli* BL21 was added for amplification of phages. Phage-infected BL21 cells were cultured in a

bacterial shaker at 37°C until lysis occurred. The amplified phage library was subtracted again using EL4 cells and B16-F10 cells and selected by incubation with BMDCs. This cycle was repeated three times. The output/input ratio was determined by counting the number of phage plaques recovered from the cells relative to the number of phages added to the cells. Single phage clones from the three round selection were amplified by *Escherichia coli* BL21 and tested for binding to BMDCs using flow cytometry. The sequences of displayed peptides were determined using specific primers for DNA encoding the insert-containing region at the C terminus of the T7 capsid protein (forward, 5-ggagctgtcgtattccagtc-3; reverse, 5-aacccctcaagacccgttta-3).

Analysis of phage binding to DCs using flow cytometry

Each phage clone was incubated with BMDCs (1×10^5 cells) in PBS containing 2% skim milk at 4°C for 1 h. After washing with PBS three times, BMDCs were incubated with anti-CD16/CD32 antibody (BioLegend, San Diego, CA, USA) and anti-T7 tail fiber monoclonal antibody (Novagen, San Diego, CA, USA) at 4°C for 30 min. After washing three times with PBS containing 1% fetal calf serum, BMDCs were incubated with biotin-labelled anti-mouse IgG2a antibody (BioLegend) at 4°C for 20 min, followed by PE-labelled streptavidin (BioLegend) at 4°C for 20 min. After washing three times with PBS containing 1% fetal calf serum, BMDCs were analyzed using flow cytometry using a NovoCyte Flow Cytometer (ACEA Biosciences, San Diego, CA, USA).

Binding assay using flow cytometry

Peptides were chemically synthesized by Scrum (Tokyo, Japan). A biotin residue was added to the N-terminus of the peptides to allow detection by PE-labelled streptavidin. AS1411 (5′-tttggtggtgg tggttgtggtggtggtgg-3′) and CRO (5′-tttcctcctcctccttctcctcctcctcct-3′) were synthesized by Hokkaido System Science (Hokkaido, Japan). Each biotin-labelled peptide (50 μg/mL for Figures 1D, 7I, and 7J, 250 μg/mL for Figures 7B and S5A, 10 μg/mL for Figures 7C, 7G, 7H, S5B, and S6B) was incubated with BMDCs (1×10^5 cells), DC2.4 cells (1×10^5 cells), or CAL-1 cells (1×10^5 cells) at 4°C for 30 min. In some cases, DC2.4 cells (1×10^5 cells) or CAL-1 cells (1×10^5 cells) were incubated with each biotin-labelled peptide in the presence of anti-NRP-1 polyclonal antibody (90 μg/mL for Figure 7B, 18 μg/mL for Figure S5A, 3.6 μg/mL for Figure S5B; R&D Systems, Minneapolis, MN, USA), control antibody (90 μg/mL for Figure 7B, 18 μg/mL for Figure S5A, 3.6 μg/mL for Figure S5B; R&D Systems), MS-3 (50 μg/mL for Figures 7H and 7J; Santa Cruz Biotechnology, Santa Cruz, CA, USA), isotype control antibody (50 μg/mL for Figures 7H and 7J; Biolegend), AS1411 (10 μM for Figures 7G and 7I), or CRO (10 μM for Figures 7G and 7I). After washing three times with PBS containing 1% BSA, 8 μg/mL of PE-labelled streptavidin was added to detect peptide binding to cells at 4°C for 30 min. After washing with PBS containing 1% BSA, the cells were analyzed using flow cytometry (NovoCyte Flow Cytometer).

Complex of neutravidin and DC-targeting peptide

We mixed 100 μg neutravidin (Sigma-Aldrich, St. Louis, MO, USA) with 166 μg of biotin-labelled peptide at 25°C for 1 h. This complex of neutravidin and peptide was purified using ultrafiltration tubes with a 10 kDa exclusion membrane (Amicon Ultra-15, Merck Millipore, Burlington, MA, USA) and used as an antigen.

Expression and purification of recombinant PspA proteins

The amino acid sequence of PspA (GenBank accession number: AF071814) was derived from the WU2 strain of *S. pneumoniae*. cDNA of PspA corresponding to amino acid residues 32–414, with an N-terminal hexahistidine tag, was cloned into a pET28a vector (Merck Millipore). The sequence of DC-targeting peptides or Tat peptide (GRKKRRQRRRPPQ) was inserted into the C-terminal of PspA. The GGGGS linker was inserted between the PspA and the DC-targeting peptide. In some cases, the sequence of Dp1 and GGGGS linker was inserted after the N-terminal hexahistidine tag. The plasmids were transformed into *Escherichia coli* BL21(DE3) cells. The expression of the PspA protein was induced by adding 0.5 mM isopropyl-β-D-1-thiogalactopyranoside and then shaken for 4 h at 37°C. After incubation, the culture medium was centrifuged at 8,000 × g for 10 min, and the pellet was suspended in a buffer containing 100 mM NaCl, 5 mM imidazole, and 20 mM Tris-HCl supplemented with protease inhibitors. BL21(DE3) cells were lysed by sonication and the soluble protein was purified from the cleared cell lysate using an AKTA explorer chromatography system with a Ni-Sepharose HisTrap FF column (GE Healthcare, Diegem, Belgium) and a Superose 6 Increase 10/300 GL column (GE Healthcare). The PspA protein was further purified using an EndoTrap® HD column (LIONEX, Braunschweig, Germany) to remove endotoxins. The level of endotoxin

in PspA (< 0.05 EU/μg) was confirmed using the Limulus Color KY Test (Wako Pure Chemical Industries, Tokyo, Japan). Recombinant PspA was quantified using Pierce BCA protein assay kit (Thermo Fisher Scientific, Hampton, NH, USA) using BSA as a standard.

Fusion of OTII or Eα with DC-targeting peptide

OTII peptide (ISQAVHAAHAEINEAGR) and OTII fusion with DC-targeting peptides was chemically synthesized by Scrum. Eα peptide (ASFEAQGALANIAVDKA) and Eα fusion with DC-targeting peptides were chemically synthesized by Scrum. During fusion with peptides, a GGGGG linker was inserted between OTII and DC-targeting peptide, or Eα and DC-targeting peptide.

Immunization

CpG ODN (K3 CpG ODN; 5-atcgactctcgagcgttctc-3) was purchased from GeneDesign (Osaka, Japan). Alhydrogel adjuvant (2% alum) was purchased from InvivoGen (San Diego, CA, USA). OVA with low endotoxin content was purchased from Fujifilm (Tokyo, Japan) and was used for immunization. Grade V OVA purchased from Sigma-Aldrich was used for ELISA. For neutravidin immunization experiment, mice were immunized with neutravidin (5 μg/mouse), neutravidin (5 μg/mouse) plus alum (250 μg/mouse), neutravidin (5 μg/mouse) plus CpG ODN (10 μg/mouse), or a complex of neutravidin and peptide (5 μg/mouse) subcutaneously at the base of the tail on days 0 and 10. For immunization with PspA, mice were immunized with PspA (1 μg/mouse), PspA (1 μg/mouse) plus alum (50 or 250 μg/mouse), PspA (1 μg/mouse) plus CpG ODN (10 μg/mouse), fusion PspA with peptide (1 μg/mouse), fusion PspA with peptide (1 μg/mouse) plus CpG ODN (10 μg/mouse), or PspA (1 μg/mouse) plus free Dp1×3 (1 μg/mouse) subcutaneously at the base of the tail on day 0, days 0 and 10, or days 0 and 21. As shown in Figure 7K, mice were immunized with PspA-Dp1×3 (1 μg/mouse) plus AS1411 (5 nmol/mouse) or PspA-Dp1×3 (1 μg/mouse) plus CRO (5 nmol/mouse) subcutaneously at the base of the tail on day 0, and mice were treated with AS1411 (5 nmol/mouse) or CRO (5 nmol/mouse) on −1 and 1 days. For immunization using OTII, mice were immunized with OTII (2 μg/mouse equivalent to 1.1 nmol/mouse), OTII (2 μg/mouse equivalent to 1.1 nmol/mouse) plus CpG ODN (50 μg/mouse), OTII-Dp1 (3 μg/mouse equivalent to 1.1 nmol/mouse), fusion OTII with peptides (5 μg/mouse equivalent to 1.1 nmol/mouse), fusion OTII with peptides (5 μg/mouse equivalent to 1.1 nmol/mouse) plus CpG ODN (50 μg/mouse), OTII-Dp1×3 (5 μg/mouse equivalent to 1.1 nmol/mouse) plus free Dp1×3 (100 μg/mouse equivalent to 4 nmol/mouse), or OTII-Dp1×3 (5 μg/mouse equivalent to 1.1 nmol/mouse) plus free Dp5×3 (100 μg/mouse equivalent to 4 nmol/mouse) subcutaneously at the base of the tail on days 0 and 10. For immunization with OVA, mice were immunized subcutaneously at the base of the tail with OVA (10 μg/mouse), OVA (10 μg/mouse) plus PspA-Dp1×3 (1 μg/mouse), or OVA (10 μg/mouse) plus alum (250 μg/mouse) on days 0 and 10. Plasma samples were collected on day 28 for mice immunized on days 0 and 21, or day 17 for mice immunized on days 0 and 10, and the plasma levels of neutravidin-, PspA-, or OVA-specific antibodies were determined using ELISA. In some cases, we obtained plasma samples several months after the second immunization. As shown in Figure 7K, plasma samples were obtained on day 20. ELISA plates were coated with neutravidin (1 μg/mL), PspA (1 μg/mL), or OVA (10 μg/mL) in 0.1 M sodium carbonate buffer (pH 9.6) overnight at 4°C. As shown in Figure 2D, the ELISA plates were coated with Dp1×3 (VSYKAIRVSYKAIRVSYKAIR: 10 μg/mL) in 0.1 M sodium carbonate buffer (pH 9.6) overnight at 4°C. The coated plates were then incubated with 1% Block Ace (DS Pharma Biomedical, Osaka, Japan) for 1 h at 25°C. Plasma samples were diluted with 0.4% Block Ace, and transferred to the antigen-coated plates. After incubation with plasma for 2 h at 25°C, the coated plates were incubated with horseradish peroxidase-conjugated goat anti-mouse IgG (Merck Millipore), IgG1 (SouthernBiotech, Birmingham, AL, USA), or IgG2c (Southern Biotech) solution for 1 h at 25°C. After incubation, the color reaction was developed with 0.8 mM tetramethyl benzidine (Dojindo, Kumamoto, Japan) in 100 mM citric acid buffer, stopped with 2 N H_2SO_4, and measured at OD450−570 on a microplate reader (Power Wave HT, BioTek, Winooski, VT, USA). For T cell analysis, spleen samples were collected on day 31, and splenocytes were prepared to determine IFN-γ production. Splenocytes (1×10^6 cells) were added to a 96-well plate and then stimulated with 50 μg/mL PspA for 1dat 37°C. After incubation, the concentrations of IFN-γ in the supernatants were analyzed using an ELISA kit (BioLegend), following the manufacturer's instructions.

Streptococcus pneumoniae challenge

Exactly 10 days after the second immunization or 21 days after the first immunization (Figure S3), mice were intranasally challenged with the WU2 strain of *S. pneumoniae*. Anesthetized mice were challenged intranasally with 1×10^7 CFU of *S. pneumoniae* in 30 μL of PBS (15 μL each). The body weights and survival rate of the challenged mice were monitored for 13 days post-challenge. The humane endpoint was set at 25%

body weight loss relative to the initial body weight at the time of infection. We defined the day that the mice had less than 75% body weight to the initial body weight as the day of death.

Stimulation of BMDCs

Mouse-derived BMDCs were seeded at a density of 1×10^5 cells/well in a 96-well flat-bottomed culture plate. The cells were treated with OTII (20 μg/mL equivalent to 11.3 nM), OTII (20 μg/mL equivalent to 11.3 nM) plus CpG ODN (10 μg/mL), OTII-Dp1×3 (50.9 μg/mL equivalent to 11.3 nM), or OTII-Dp2×3 (46.3 μg/mL equivalent to 11.3 nM) for 24 h at 37°C. Supernatants were analyzed using ELISA kits to determine the concentrations of IL-6 (BioLegend) and IL-12 p40 (BioLegend), according to the manufacturer's instructions.

Biodistribution of Dp1 *in vivo*

Mice were treated with TAMRA-labelled trimeric Dp1 (10 μg equivalent to 3.5 nmol/mouse) or TAMRA-labelled trimeric Dp2 (8.6 μg equivalent to 3.5 nmol/mouse) subcutaneously at the ear. Exactly 24 h after treatment, the draining lymph nodes were collected. To prepare single-cell suspensions, we incubated the draining lymph nodes with 200 μg/mL Liberase TL (Roche Diagnostics GmbH, Mannheim, Germany) and 10 U DNaseI (Roche Diagnostics GmbH) for 1 h at 37°C. To separate various subsets of APCs from the collected cells, we incubated the cells with Fixable Viability Dye eFluor™ 780 (eBioscience, San Diego, CA, USA), anti-CD16/CD32 antibody (BioLegend), APC-labelled anti-mouse PDCA-1 antibody (BioLegend), PerCP/Cy5.5-labelled anti-CD11c antibody (BioLegend), BV421-labelled anti-I-A/I-E antibody (BioLegend), and Alexa Fluor 700-labelled anti-mouse CD19 antibody (BioLegend). The cells were then analyzed using flow cytometry using a Attune NxT Flow Cytometer (Thermo Fisher Scientific). The cultured cells were classified into the following subsets: PDCA-1$^-$ I-A/I-E$^+$ CD11c^{high} cDCs, PDCA-1$^-$ I-A/I-E^{high} CD11c$^+$ mDCs, PDCA-1$^-$ I-A/I-E$^+$ CD11c$^-$ CD19$^+$ B cells, and PDCA-1$^-$ I-A/I-E$^+$ CD11c$^-$ CD19$^-$ macrophages.

Antigen presentation on APCs *in vivo*

C57BL/6J mice were treated with Eα (30 μg equivalent to 18 nmol/mouse), Eα-Dp1×3 fusion (79 μg equivalent to 18 nmol/mouse), or Eα-Dp2×3 fusion (72 μg equivalent to 18 nmol/mouse) subcutaneously at the ear. On days 1, 3, and 5 after administration, draining lymph nodes were collected. To prepare single-cell suspensions, we incubated the draining lymph nodes with 200 μg/mL Liberase TL and 10 U DNaseI for 1 h at 37°C. Eα presentation on I-Ab, which is MHC class II, was detected using biotin-labelled anti-I-Ab:Eα complex-specific antibody, YAe (eBioscience), and PE-labelled streptavidin. We separated various subsets of APCs as described above.

Binding of DC-targeting peptides to NRP-1 protein

Approximately 10 μg (equivalent to 28 pmol) of PE-labelled streptavidin was mixed with 2.8 nmol biotin-labelled DC-targeting peptide for 1 h at 25°C. The PE-labelled streptavidin and peptide complex was purified using an ultrafiltration tube. White OptiPlate-96 (Perkin-Elmer, Norwalk, CT, USA) was coated with 10 μg/mL recombinant mouse NRP-1 protein (R&D Systems) in 0.1 M sodium carbonate buffer (pH 9.6) overnight at 4°C. The coated plates were washed with PBS containing 0.05% Tween-20 and incubated with PBS containing 1% BSA for 1 h at 25°C. After washing, the plates were incubated with PE-labelled streptavidin and peptide complex for 2 h at 25°C. After washing the plates, fluorescence was measured using a multi-plate reader (DS Pharma Biomedical).

Suppression of NRP1 expression using siRNA

DC2.4 cells (4×10^4 cells) were cultured in 96-well plates for 12 h at 37°C. The cells were further incubated with 10 μM NRP-1 siRNA (5'-ctgctacttcacagtatggta-3') and 0.4 μL Lipofectamine 3000 reagent (ThermoFisher) for 48 h at 37°C. Subsequently, the cells were collected and analyzed for NRP-1 expression and Dp1 binding using flow cytometry. NRP1 expression was evaluated using Fixable Viability Dye eFluor™ 780 and BV421-labelled anti-mouse CD304 (Neuropilin-1) antibody (BioLegend).

Recombinant nucleolin protein

A cDNA of murine nucleolin (GenBank accession number: X07699.1) corresponding to amino acid residues 309–644 was cloned into the pGEX-6P-2 vector (Merck Millipore). Transformed BL21 (DE3) cells were grown at 37°C to an OD600 of 0.5. Protein expression was induced by adding 0.2 mM isopropyl-β-D-1-thiogalactopyranoside followed by shaking for 4 h at 37°C. After incubation, bacteria were pelleted by centrifugation

at 8,000 × *g* for 10 min; the pellet was resuspended in a buffer containing 100 mM NaCl, 5 mM imidazole, and 20 mM Tris-HCl supplemented with protease inhibitors. The bacteria were lysed by sonication. Soluble protein was purified from the cleared cell lysate using an AKTA explorer chromatography system with a Ni-Sepharose HisTrap FF column and a Superose 6 Increase 10/300 GL column. Recombinant nucleolin was quantified using a Pierce BCA protein assay kit with a BSA standard.

Binding of peptides and AS1411 to recombinant nucleolin protein

White OptiPlate-96 (Perkin-Elmer, Norwalk, Connecticut, USA) microplates were coated with 10 μg/mL recombinant nucleolin protein or 10 μg/mL OVA in carbonate buffer overnight at 4°C. The coated plates were washed with PBS containing 0.05% Tween-20 and incubated with PBS containing 1% BSA for 1 h at 25°C. After washing, 10 μg/mL of biotin-labelled Dp1×3 or biotin-labelled Dp2×3 was incubated for 1 h at 25°C, followed by PE-labelled streptavidin for 2 h at 25°C. In the other experiment, the plates were incubated with 0.5 μM biotin-labelled AS1411 in the presence or absence of 100 μg/mL Dp1×3 or Dp2×3, then with PE-labelled streptavidin for 2 h at 25°C. After washing the plates, fluorescence was measured using a multiplate reader (DS Pharma Biomedical, Osaka, Japan).

Affinity chromatography

Mouse-derived BMDCs (5 × 10^7 cells) were lysed in 10 mM HEPES-NaOH (pH 7.9), 10 mM KCl, 0.1 mM EDTA, 1 mM DTT, and 1% NP-40. Approximately 1 mg of HM-NeutrAvidin beads (Tamagawa Seiki, Nagano, Japan) were incubated with 10 mM biotin-labelled Dp1 or biotin-labelled Dp5 at 4°C for 1 h. After centrifugation, peptide coated-HM-NeutrAvidin beads were incubated with cell lysate at 4°C for 2 h in 20 mM HEPES-NaOH (pH 7.9), 100 mM KCl, 1 mM $MgCl_2$, 0.2 mM $CaCl_2$, 0.2 mM EDTA, 10% glycerol, and 1mM DTT, according to the manufacturer's instructions. After centrifugation, bound proteins were eluted with 0.1 M glycine-HCl (pH 2.5) and separated using SDS-PAGE. Gel fragments excised from Lumitein (Biotium, Fremont, CA, USA)-stained gel of eluted fractions were subjected to LC-MS/MS at the Central Instrumentation Laboratory, Research Institute for Microbial Diseases, Osaka University.

Expression level of cell-surface nucleolin on DCs

To examine the expression level of cell surface nucleolin on DCs, DC2.4 cells (1 × 10^5 cells) and mouse-derived BMDCs (1 × 10^5 cells) were incubated with 0.1 μM biotin-labelled AS1411 or 0.1 μM CRO, and 8 μg/mL PE-labelled streptavidin was added to detect AS1411 or CRO binding to cells at 4°C for 30 min. After washing with PBS containing 1% BSA, the cells were analyzed using flow cytometry.

QUANTIFICATION AND STATISTICAL ANALYSIS

Statistical analyses

Statistical analyses were performed using Prism software (GraphPad Software, San Diego, CA, USA). All data are presented as the mean ± standard deviation (SD). Significant differences were determined using Tukey's test or Student's *t*-test. Significant differences in survival rates were obtained by comparing the Kaplan–Meier curves using the log-rank test. Statistical significance was set at $p < 0.05$.